https://doi.org/10.5194/egusphere-2023-1348
Preprint. Discussion started: 20 July 2023

Comparison of the H_2O, HDO and δD stratospheric climatologies between the MIPAS-ESA v8, MIPAS-IMK v5 and ACE-FTS v4.1/4.2 satellite data sets

Karen De Los Ríos[1,2], Paulina Ordoñez[3,2], Gabriele P. Stiller[4], Piera Raspollini[5], Marco Gai[5], Kaley A. Walker[6], Cristina Peña-Ortiz[3], and Luis Acosta[1]

[1]Instituto de Física, Universidad Nacional Autónoma de México, Mexico City, 04510, Mexico
[2]Instituto de Ciencias de la Atmósfera y Cambio Climático, Universidad Nacional, Mexico City, 04510, Mexico
[3]Departamento de Sistemas Físicos, Químicos y Naturales, Universidad Pablo de Olavide, Sevilla, Spain
[4]Karlsruhe Institute of Technology, Institute for Meteorology and Climate Research, Hermann-von-Helmholtz-Platz 1, 76344 Leopoldshafen, Germany
[5]Istituto di Fisica Applicata "Nello Carrara" (IFAC) del Consiglio Nazionale delle Ricerche (CNR), Florence, Italy
[6]University of Toronto, Department of Physics, 60 St. George Street, Toronto, Ontario M5S1A7, Canada

Correspondence to: L. Acosta (acosta@fisica.unam.mx)

Abstract. Variations in the isotopological composition of water vapour are fundamental for understanding the relative importance of different mechanisms of water vapor transport from the tropical upper troposphere to the lower stratosphere. Previous comparisons obtained from observations of H_2O and HDO by satellite instruments showed discrepancies. In this work, newer versions of H_2O and HDO retrievals from Envisat/MIPAS are compared with data derived from SCISAT/ACE-FTS. Specifically, MIPAS-IMK V5, MIPAS-ESA V8, and ACE-FTS V4.1/4.2 for the common period from February 2004 to April 2012 are compared for the first time through a profile-to-profile approach and comparison based on climatological structures. Stratospheric H_2O and HDO global average coincident profiles reveal good agreement. The smallest biases are found between 20 and 30 km, and the largest biases are exhibited around 40 km both in absolute and relative terms. For HDO, biases between -8.6-10.6 % are observed among the three databases in the altitudes of 16 to 30 km. However, around 40 km, ACE-FTS agrees better to MIPAS-IMK than MIPAS-ESA, with biases of -4.8% and -37.5%, respectively. The HDO bias between MIPAS-IMK and MIPAS ESA is 28.1 % at this altitude. The meridional cross-sections of H_2O and HDO exhibit the expected distribution that has been established in previous studies. The tape recorder signal is present in H_2O and HDO for the three databases with slight quantitative differences. The meridional cross-sections of δD are in good agreement with the previous version of MIPAS-IMK and ACE-FTS data. In the temporal δD variations, the results suggest that in the current data versions, the calculated isotopic composition (δD) from MIPAS-IMK aligns more closely with expected stratospheric behavior for the entire stratosphere. Nevertheless, there are differences in the climatological δD composites between databases that could lead to different interpretations regarding the water vapor transport processes toward the stratosphere, so it is important to intercompare these δD observations.

https://doi.org/10.5194/egusphere-2023-1348
Preprint. Discussion started: 20 July 2023

1. INTRODUCTION

Water vapour (WV) is the most important non-anthropogenic greenhouse gas in Earth's atmosphere (Hegglin et al., 2014). Although WV concentration is much lower in the stratosphere than in the troposphere, it significantly affects the climate at the surface (Solomon et al., 2007). Stratospheric water vapour (SWV) affects atmospheric dynamics and thermodynamics by modulating the radiative forcing directly (e.g., Solomon et al., 2010; Riese et al., 2012) and indirectly through its effect on the stratospheric ozone chemistry (Vogel et al., 2011). Moreover, it has been shown that the cold point temperature in the tropics is expected to rise in the future which will lead to increasing SWV due to reduced freeze-drying in the tropical tropopause layer (TTL; Gettelman et al., 2009). This implies the existence of a SWV feedback (Dessler et al., 2013; Banerjee et al., 2020).

The humidity in the lower stratosphere has been increasing in the last decades. Scientists discovered it at the beginning of the century. However, the reason for this humidification was not understood (Rosenlof et al., 2001). Because of the number of atmospheric composition measurement instruments that have been implemented on satellites over the past several decades, studies related to the SWV transport process have been increasing (e.g., Mote et al., 1996; Steinwagner et al., 2007; Lossow et al., 2011; Randel et al., 2012; Scheepmaker et al., 2016; Schneider et al., 2020). Brewer-Dobson circulation (Brewer, 1949) transports H_2O-rich air through upwelling from low tropospheric latitudes, accompanied by large horizontal motions to mid-stratospheric latitudes. WV is also produced in the middle atmosphere through methane oxidation and is destroyed through photodissociation and reactions with O(1D) (Wang et al., 2018). However, the observed variability in SWV concentrations cannot be fully explained by observed changes in these main drivers (Hegglin et al., 2014). Therefore, studies focused on the dynamical processes that determine SWV variability constitute an active contemporary area of research (Plaza et al., 2021).

One way to conduct studies of troposphere-stratosphere mass transport is through isotopologues related to these species that behave as phenomenological tracers (Kuang et al., 2003). The isotopological composition of WV in the stratosphere provides an observational constraint for determining the relative importance of the possible transport mechanisms (Payne et al., 2007). Among the isotopological species of WV, $HD^{16}O$ (hereafter HDO) is particularly useful due to its significant fractionation effect (Merlivat and Nief, 1967; Kuang et al., 2003). Therefore, the analysis of HDO at the tropopause is a very useful tracer to diagnose the relative importance of slow ascent and convective ice-lofting for WV transport into the stratosphere (Moyer et al., 1996; Tuinenburg et al., 2015; Wang et al., 2019).

Satellite remote sounding of the Earth's limb is currently the only method of observing the atmosphere that allows near-global time series of atmospheric profiles to be obtained from the upper troposphere to the lower thermosphere (Sheese et al., 2017). However, each atmospheric measurement with this method has its sources of uncertainty and systematic biases, which must be examined. Limb earth probing instruments may exhibit other systematic differences from similar devices depending on the observed latitudinal region and/or the observed local time. In addition to the differences due to each molecule‘s volume mixing

https://doi.org/10.5194/egusphere-2023-1348
Preprint. Discussion started: 20 July 2023

ratio (VMR) retrieval algorithms, these biases must also be characterized. Sometimes, even significant discrepancies between data retrieved from the same satellite can be found depending on the algorithm.

There are different datasets of WV and its isotopologues in the stratospheric region, retrieved mainly from three instruments. One of them, the Odin satellite, carries a Sub-Millimetre Radiometer (SMR), observing stratospheric H_2O, $H_2{}^{18}O$, and HDO (Murtagh et al., 2002). For technical reasons (the maximum bandwidth of a single radiometer is only 0.8 GHz), and H_2O and HDO cannot be measured simultaneously (Wang et al., 2018). Therefore, this study is focused on the other two instruments.

The instrument MIPAS (Michelson Interferometer for Passive Atmospheric Sounding; Fischer et al., 2008) aboard Envisat (Environmental Satellite) was launched in 2002 and ceased operation in 2012 when contact with the satellite was lost. This instrument makes highly reliable WV observations in the stratosphere (Payne et al., 2007; von Clarmann et al., 2009; Ceccherini et al., 2011). On the other hand, the instrument ACE-FTS (Atmospheric Chemistry Experiment - Fourier Transform Spectrometer; Bernath et al., 2005; Nassar et al., 2005) that yields WV information in the stratosphere to the present day (Boone et al., 2020) is aboard the Canadian satellite SCISAT, which was launched in 2003.

In the case of MIPAS, different retrievals methods have been developed. One of the data sets, named here MIPAS-IMK, was retrieved with the IMK/IAA processor, which was developed in collaboration between the "Institut für Meteorologie und Klimaforschung" (IMK) in Karlsruhe, Germany, and the "Instituto de Astrofísica de Andalucía" (IAA) in Granada, Spain (see for general description, e.g. Högberg et al., 2019; Lossow et al., 2019; Lossow et al., 2020; Hegglin et al., 2013). The other MIPAS dataset, named here MIPAS-ESA V8 products (Dinelli et al. 2021), was retrieved by using the Optimized Retrieval Model (ORM) algorithm (Raspollini et al., 2022 and references therein) on the full-mission reprocessing campaign performed on L1V8 (Kleinert et al., 2018). The ACE-FTS retrievals have evolved through several versions with the retrieval model being updated with optimized parameters (Boone et al., 2005, 2013, 2020). In this work, we evaluate H_2O and HDO data sets derived from observations by MIPAS-IMK V5H and V5R, MIPAS-ESA level 2 V8.0, and ACE-FTS V4.1/4.2 for the common period from February 2004 to April 2012.

WV observations have been collectively evaluated through a multitude of parameters, like biases, drifts or variability characteristics, correlations, and other statistical data by the WCRP/SPARC water vapor assessment II (WAVAS-II) activity (https://amt.copernicus.org/articles/special_issue10_830.html). The last evaluation of Lossow et al. (2019) used ACE-FTS v3.5 (2004-2014), MIPAS-ESA V5H (2002-2004), and MIPAS-ESA V7R (2005-2012), MIPAS-IMK V5H (2002-2004) version 20 and V5R (2005-2012) version 220/221. In this work, we use newer versions of some H_2O data sets than those employed in the previous studies, including MIPAS-ESA v8 and ACE-FTS v4.1/4.2, whose improvements will be described in the next section.

https://doi.org/10.5194/egusphere-2023-1348
Preprint. Discussion started: 20 July 2023

Regarding HDO, Lossow et al. (2011) compared HDO data from MIPAS Level-1 retrieved with IMK/IAA processor (data version 20), SMR from Odin version 2.1, and ACE-FTS 2.2, and they found good general agreement. However, distinct observational discrepancies of the δD (see section 3.2) annual variation were visible between MIPAS-IMK (Steinwagner et al., 2010) and ACE-FTS (Randel et al., 2012) data. Lossow et al. (2020) reassessed the discrepancies based on MIPAS-IMK and ACE-FTS data sets. Overall, the used data set covered the period from July 2002 to March 2004, which is referred to as the full resolution period of MIPAS (Lossow et al., 2020). However, a longer time series is needed to draw robust conclusions on the relative importance of different mechanisms transporting WV into the stratosphere. Therefore, we focus here on newer data versions that cover the full mission period of ten years These data versions were first published by Speidel et al. (2018) and not yet compared to other observations. For HDO MIPAS-ESA, there are no published comparisons yet.

We compare the three H_2O and HDO observation databases relying on two approaches. First, we present profile-to-profile comparisons and provide a general overview of the typical biases in the observational databases. The second approach is based on climatological comparisons, including meridional cross sections and time series comparisons. Section 2 describes the individual data sets in detail. In section 3, the methodology is outlined. Section 4 presents the results, which will be summarised in section 5.

2. DATA SETS

As mentioned in the introduction, we employ newer data sets than those used in the previous studies. Here, we employ the MIPAS-IMK V5H_H2O_20 (2002-2004) and V5R_H2O_220/221 (2005-2012) for H_2O case, and MIPAS-IMK V5H_HDO_22 (2002-2004) and V5R_HDO_222/223 (2005-2012) for HDO (Speidel et al., 2018), the MIPAS ESA Level 2 V8 dataset (Dinelli et al., 2021) results from the full-mission reprocessing campaign performed on L1V8 products and ACE-FTS v4.1/v.2 (Boone et al., 2020) for both isotopologues.

2.1. MIPAS

MIPAS was a cooled, high-resolution Fourier transform spectrometer aboard Envisat (Fischer et al., 2008). Envisat was launched on 1 March 2002 and made observations until 8 April 2012, when communication with the satellite was lost. Envisat orbited the Earth 14 times a day in a sun-synchronous polar orbit at about 790 km altitude. The equator crossing times were 10:00 and 22:00 local time for the descending and ascending nodes, respectively. MIPAS measured the thermal emission of the atmospheric limb, covering all latitudes. MIPAS operated at 100 % of its duty cycle from July 2002 to March 2004, when, due to a significant anomaly affecting the Interferometer Drive Unit (IDU), its regular operations were interrupted to avoid the mechanical blockage of the instrument (Dinelli et al., 2021). After various tests with different spectral resolutions, the European Space Agency (ESA) recovered the instrument in January 2005 at a reduced spectral resolution but a finer vertical sampling.

https://doi.org/10.5194/egusphere-2023-1348
Preprint. Discussion started: 20 July 2023

At the beginning of 2005, MIPAS operated at only a 30 % duty cycle, which progressively increased until December 2007, when it was successfully restored to 100 % operations (Kleinert et al., 2007, 2018).

2.1.1. MIPAS-IMK

MIPAS-IMK database is obtained from the collaboration between IMK and IAA with the algorithm that they developed for the retrieval of VMR that produces level 2 data (von Clarmann et al., 2009). The IMK-IAA algorithm uses a non-linear least-squares global-fitting technique with Tikhonov regularisation, which is a constrained iterative inversion technique. Small spectral regions, so-called microwindows, are used where the respective species have suitable spectral lines. The data are retrieved on a 1 km grid, and the efficiency-dependent strength of the smoothing constraint was chosen to optimize vertical resolution while limiting unphysical oscillations in the retrieved profile. MIPAS-IMK WV retrievals are performed in $\log(VMR)$ space (see e.g., the SPARC-WAVAS-II Special issue (https://amt.copernicus.org/articles/special_issue10_830.html) for validation of this data version. The HDO data version used here differs significantly from the data versions assessed by Lossow et al. (2020) and Högberg et al. (2019) and used by Steinwagner et al. (2007, 2010). For the data version used here, HDO was retrieved in linear space with the previously retrieved main isotopologue profile as a priori information. δD (see section 3.2) is calculated from the regular water vapour product and HDO; by this the disadvantage of using a less-than-optimal data version of H_2O is omitted, and the vertical resolution of δD is provided by the difference of the a priori and retrieved profile (Speidel et al., 2018).

2.1.2. MIPAS-ESA

The MIPAS ESA Level 2 V8 dataset (Dinelli et al., 2021) results from the full-mission reprocessing campaign performed on L1V8 products using the Optimized Retrieval Model (ORM) processor version 8.22 (Raspollini et al., 2022) funded by the European Space Agency (ESA). The algorithm fits forward-model spectra to measured infrared spectra in species-dependent micro-windows via least-squares global fitting, using the Gauss-Newton approach modified with the Levenberg-Marquardt method to minimize the fit residual. For H_2O a posteriori regularisation is applied with a retrieval error-dependent regularisation strength (Ridolfi and Sgheri, 2011). For HDO, retrieval is performed with Optimal Estimation, with the a priori profile equal to the retrieved H_2O profile, opportunely scaled according to the constant value of the HDO isotopic abundance (3.107×10^{-4}), provided by the HITRAN spectroscopic database. The diagonal elements of the covariance matrix of the a priori are computed as the square of the sum of a constant (10^{-3} ppmv) plus the 100% of the a priori profile, while the non-diagonal elements are computed assuming a correlation length of 10 km.

The forward model used in the algorithm accounts for horizontal inhomogeneities of temperature and trace species and assumes that the atmosphere is in local thermodynamic equilibrium (LTE).

https://doi.org/10.5194/egusphere-2023-1348
Preprint. Discussion started: 20 July 2023

2.2. ACE-FTS

ACE-FTS is one of three instruments aboard the Canadian satellite SCISAT (Bernath et al., 2005). SCISAT was launched on the 12 August 2003 into a highly inclined, 74°, orbit at 650 km altitude. This orbit provides latitudinal coverage of 85° S to 85° N but is optimized for observations at high and middle latitudes. ACE-FTS scans the Earth's atmosphere during up to 15 sunrises and 15 sunsets daily from approximately 5 to 150 km altitude. Vertical sampling varies with altitude and orbit beta angle, from around 1 to 2 km in the upper troposphere through approximately 6 km in the upper stratosphere and mesosphere. HDO information is retrieved from two spectral bands: 3.7 to 4.0 µm (2493-2673 cm^{-1}) and 6.6 to 7.2 µm (1383-1511 cm^{-1}). H_2O retrieval uses spectral information between 3.3 and 10.7 µm (937-2993 cm^{-1}) (Lossow et al., 2020).

Here, we use ACE-FTS version 4.1/4.2. The ACE-FTS trace species VMR retrieval algorithm is described by Boone et al. (2005, 2013), and the changes for the most recent version of the retrieval v4.1/4.2 are Boone et al. (2020). The retrieval algorithm uses a non-linear least-squares global-fitting technique that fits the ACE-FTS observed spectra in given micro-windows to forward modelled spectra-based on line strengths and line widths from the HITRAN 2016 database (with updates as described by Gordon et al. (2017)). The pressure and temperature profiles used in the forward model are the ACE-FTS derived profiles, calculated by fitting CO_2 lines in the observed spectra. The version 4.1/4.2 retrieval grid uses a minimum altitude spacing of 2 km for tangent heights above 15 km and a minimum spacing of 1 km for tangent heights below 15 km. This limitation on the retrieval grid suppresses unphysical oscillations that commonly occurred above 15 km in previous processing versions when the tangent height spacing dropped below 2 km. The main changes made in the v4 retrievals are amended micro windows for most species that allow for a more significant number of interfering species; improvements to the temperature and pressure retrievals, leading to fewer unnatural oscillations in the vertical profiles (Sheese et al., 2017).

3. METHODS

All data used here were managed in agreement with the user manuals of each dataset. For MIPAS-IMK, we followed Lossow et al. (2020) and Högberg et al. (2019). For ACE-FTS, we used the specifications given by Sheese et al. (2015) and Boone et al. (2020), and Dinelli et al. (2021) was employed for MIPAS-ESA. The present quality assessment of H_2O and HDO data mainly focuses on the stratosphere, although data for the upper troposphere and lower mesosphere are used if available. The data quality assessment process is performed for H_2O and HDO from the three databases.

3.1. Profile to profile comparisons

We use the profile-to-profile comparison approach proposed by Högberg et al. (2019), where each profiles was interpolated on a common regular pressure grid, defined as the height vector of MIPAS-IMK since 1 to 70 km.

https://doi.org/10.5194/egusphere-2023-1348
Preprint. Discussion started: 20 July 2023

3.1.1 Coincidences

The global observations are considered to be coincident when they meet the following criteria (Högberg et al., 2019):

- Spatial separation of less than 1000 km.
- Temporal separation less than 24 h.
- Geolocation separation less than 5º, both in longitude and equivalent latitude.

For the final coincidence pairs, the ACE-FTS data, which is the sparser dataset was used as the first data set in all comparisons to avoid inconsistent results. Figure 1 shows a map for all ACE-FTS and MIPAS-IMK coincident profiles (Fig. 1(a)) and ACE-FTS and MIPAS-ESA coincident profiles (Fig. 1(b)) between 25-27 July 2010. Figure 1 illustrates that for each ACE-FTS profile (black circles), there two or three MIPAS-IMK (blue crosses) and MIPAS-ESA (red crosses) profiles that meet the coincidence criteria. This is because the horizontal difference between two MIPAS profiles is appr. 400 km, i.e., two to three profiles fall into the coincidence radius. The corresponding values are arithmetically averaged if multiple coincidences are found in coincident regions, generating a single point. One observation from ACE can be found to be coincident with other MIPAS observations. In the comparisons between MIPAS instrument databases, we have chosen MIPAS-ESA as the reference database. It should be mentioned that the coincident profiles from ESA and IMK are not necessarily the same because of profiles potentially not available due to convergence issues in the retrieval, or due to flags filtering out different profiles.

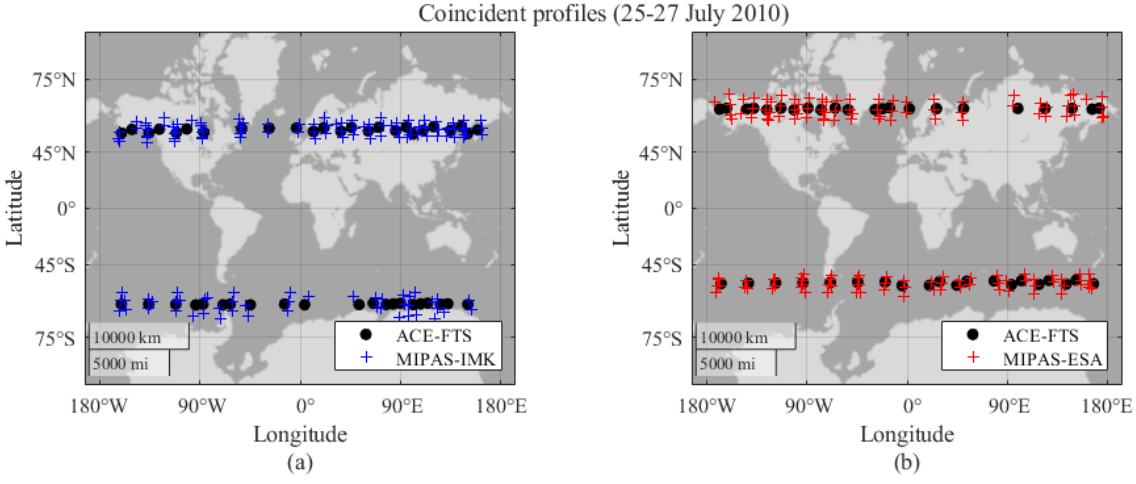

Figure 1: Coincident profiles between (a) ACE-FTS and MIPAS-IMK and (b) ACE-FTS and MIPAS-ESA on 25-27 July 2010. Different markers indicate the database, ACE-FTS (black circles), MIPAS-IMK (blue crosses), and MIPAS-ESA (red crosses).

https://doi.org/10.5194/egusphere-2023-1348
Preprint. Discussion started: 20 July 2023

The profiles from each dataset were linearly interpolated for the comparisons onto a 58 level grid between 0 to70 km, which are the altitude reference levels of MIPAS-IMK as described by Lossow et al. (2011). Then, the mean is computed as the arithmetical average of the data distribution for each altitude level and the data dispersion is obtained by standard deviation.

3.1.2. Comparison of vertical profiles

Once the orbits of the coincident profiles have been obtained, the global average altitude profiles are determined. Fig. 2(a) and Fig. 2(b) show the number of matched profiles by altitude between ACE-FTS and MIPAS-IMK and ACE-FTS and MIPAS-ESA, respectively. In both cases, the number of valid matches increases in the UTLS, and more than 40,000 matched profiles are obtained from the mid-stratosphere and upwards.

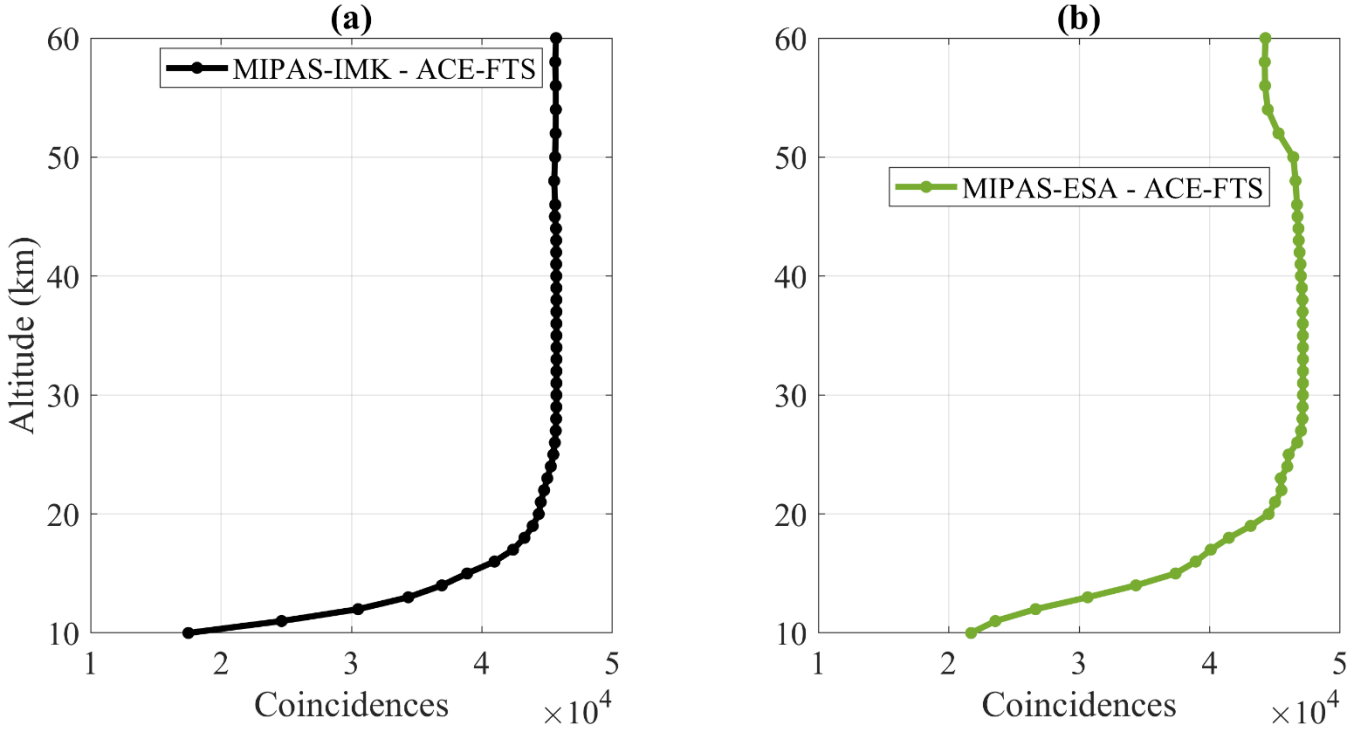

Figure 2: The global number of coincident sets of data (2004-2012) for (a) MIPAS-IMK and ACE-FTS and (b) MIPAS-ESA and ACE-FTS comparisons.

3.1.3. Bias determination

Four statistical parameters have been calculated for the globe at each altitude level: mean absolute biases, mean relative biases, the debiased standard deviation of the relative biases, and Pearson correlation coefficient for three of the six possible

https://doi.org/10.5194/egusphere-2023-1348
Preprint. Discussion started: 20 July 2023

comparisons in pairs of data. These evaluations follow the methodology used in previous assessments (Lossow et al., 2019, Högberg et al., 2019, Wetzel et al., 2013) and follow the recommendations of Loew et al. (2017).

(a) The mean absolute bias: the bias between two coincident data sets for a specific altitude level and for a given isotopologue I (i.e., HDO, H_2O), has been calculated as:

$$\overline{b_{abs}}(I,\theta,z,t) = \frac{1}{n}\sum_{i=1}^{n} b_i(I,\theta,z,t) \ , \quad (1)$$

where n denotes the corresponding number of coincident measurements, θ the latitude, z the altitude, t the period and $b_i(I,\theta,z,t)$ are the individual differences between them. These differences are considered as:

$$b_i(I,\theta,z,t) = x_i(I,\theta,z,t)_1 - x_i(I,\theta,z,t)_2 \ , \quad (2)$$

where $x_i(I,\theta,z,t)_1$ are the individual H_2O or HDO abundances of the first data set and $x_i(I,\theta,z,t)_2$ are the abundances of the second data set that are compared.

(b)The mean relative bias: this is calculated by dividing the mean absolute bias by the mean reference value (Wetzel et al., 2013).

$$\overline{b_{rel}}(I,\theta,z,t) = \frac{\overline{b_{abs}}(I,\theta,z,t)}{\frac{1}{n}\sum_{i=1}^{n} x_{ref}(I,\theta,z,t)}. \quad (3)$$

For the reference value, different options are possible (e.g., Randall et al., 2003; Dupuy et al., 2009). The mean of the two datasets have been chosen because the satellite observations can have large uncertainties, and thus the mean is an appropriate approach (Lossow et al., 2019):

$$x_{ref}(I,\theta,z,t) = \frac{x_1(I,\theta,z,t)+x_2(I,\theta,z,t))}{2} \ . \quad (4)$$

(c) Debiased standard deviation: The debiased standard deviation ($\sigma_{\overline{b}}$) is represented by the standard deviation of the mean bias-corrected between the two sets of compared data:

$$\sigma_{\overline{b}}(I,\theta,z,t) = \sqrt{\frac{1}{n-1}\sum_{i=1}^{n}\left(b_i(I,\theta,z,t) - \overline{b(I,\theta,z,t)}\right)^2} \quad (5)$$

https://doi.org/10.5194/egusphere-2023-1348
Preprint. Discussion started: 20 July 2023

This quantity measures the precision of the two data sets being compared, particularly in cases where a complete evaluation of the random error budget is not available for all the instruments involved (von Clarmann et al., 2006).

(d) Pearson correlation coefficient: the correlation coefficient r dependent on altitude levels is defined as:

$$r(I,\theta,z,t) = \frac{1}{n-1}\sum_{i=1}^{n}\left(\frac{x_i(I,\theta,z,t)_1 - \overline{x(I,\theta,z,t)_1}}{\sigma_{x_1}}\right)\left(\frac{x_i(I,\theta,z,t)_2 - \overline{x(I,\theta,z,t)_2}}{\sigma_{x_2}}\right) \quad (7)$$

We use this standard methodology because the quantity of data is large in all cases, and then the data distribution behaves as a normal distribution, resulting in a robust correlation coefficient (Lanzante, 1996).

$\overline{b_{abs}}$, $\overline{b_{rel}}$, $\sigma_{\overline{b}}$ and r were calculated at each altitude level in pairs with the combination of ACE-FTS- minus MIPAS-IMK, ACE-FTS minus MIPAS-ESA, and MIPAS-ESA minus MIPAS-IMK data set for the coincident profiles (Steinwagner et al., 2007; Toohey and Strong, 2007).

3.2. Other comparisons as a function of space and time

Here we compare the climatologies of H_2O, HDO, and the isotopic ratio between HDO and H_2O, typically noted by δD. In this approach, each grid box represents an average over several measurements. It has the advantage of not requiring coincidences. Therefore, the databases are larger, but the weakness is that sampling biases can affect the comparison.

We first performed the data binning. $x_i\ (I,\bar{\theta},\bar{\phi},t,z)$ is the individual concentration of the isotopologue $I\ (H_2O\ or\ HDO)$ for a given time t, a latitude $\bar{\theta}$, a longitude $\bar{\phi}$ and for an altitude z. We average the data sets that match the condition for belonging to a given bin.

$$I_{\overline{VMR}}(I,\bar{\theta},\bar{\phi},t,z) = \frac{1}{n_o}\sum_{i=1}^{n_o} x_i(I,\bar{\theta},\bar{\phi},t,z) \quad (8)$$

where n_o is the amount of data found within the established grid, and $I_{\overline{VMR}}$ is the value representing all the data fulfilling the grid condition (Högberg et al., 2019).

Using the results of the procedure described before, we assessed the isotopic composition through the expression $R = \frac{[D]}{[H]}$ that can be determined through the concentration of the isotopologues of water as follows:

https://doi.org/10.5194/egusphere-2023-1348
Preprint. Discussion started: 20 July 2023

$$\frac{[D]}{[H]} = \frac{[HDO]+2[DDO]}{2[H_2O]+[HDO]} \approx \frac{[HDO]}{2[H_2O]} \quad . \tag{9}$$

To quantify the abundances of heavy isotopes, R is usually compared to a standard reference ratio known as R_{VSMOW} through the following relationship:

$$\delta D = \left(\frac{R}{R_{VSMOW}} - 1\right) \times 1000 \tag{10}$$

where VSMOW=155.76 x 10^{-6} is the reference ratio (Vienna Standard Mean Ocean Water; Hagemann et al., 1970). Using Eq. (9) and Eq. (10), it is possible to obtain the deuterium excess as:

$$\delta D_{\overline{VMR}}(\delta D, \bar{\theta}, \bar{\phi}, t, z) = \left[\frac{HDO_{\overline{VMR}}(HDO, \bar{\theta}, \bar{\phi}, t, z)}{2 \cdot VSMOW \cdot H_2O_{\overline{VMR}}(H_2O, \bar{\theta}, \bar{\phi}, t, z)} - 1\right] \cdot 1000. \tag{11}$$

From the grid box means of H_2O, HDO and δD, several climatologies are compared for the period 2004-2012.

Latitude cross sections comparison is a method for comparing climatologies. The latitude bins were $\Delta\bar{\theta}$=10° and we focused on two different seasons: December-February (DJF) and June-August (JJA).
Examining time series is another way to compare the data. The time series used in this section are based on zonal means obtained considering the latitude range from 30º S to 30º N. This comparison shows how each database captures seasonal cycles and interannual variability. The maps and graphics are smoothed via the smooth function in MATLAB R2021a.

4. RESULTS AND DISCUSSION

4.1. Vertical profiles comparisons

The global average H_2O profiles for ACE-FTS compared to MIPAS-IMK and to MIPAS-ESA are shown in Figs. 3(a) and 3(c), respectively. The error bars given for the average profiles are the 1-σ standard deviation of the distribution of measurements at each altitude level. The vertical coincident profiles of H_2O exhibit a slight increase with altitude in the stratosphere (from 15 km up to 50 km, approximately) both for MIPAS-IMK and MIPAS-ESA, which is consistent with the stronger chemical generation of WV through methane oxidation in the upper stratosphere near 50 km (LeTexier et al., 1988). Similar coincident profiles are obtained for ACE-FTS in the tropical lower stratosphere (below 30 km). In fact, profiles between the 20 and 30 km levels are almost the same for ACE-FTS and MIPAS-IMK (Fig. 3(a)). The higher values of MIPAS-IMK in the tropopause region are due to the limited vertical resolution in these levels as indicated in previous works (Hegglin et al., 2013) (Fig. 3(a)). In ACE-FTS, the decrease of the mean WV concentration with altitude is less pronounced in the upper

https://doi.org/10.5194/egusphere-2023-1348
Preprint. Discussion started: 20 July 2023

stratosphere and the lower mesosphere (Figs. 3(a) and 3(c)). However, the dispersion of the data around the measure of mean indicates that the data between 12 to 30 km are comparable in the three databases. Högberg et al. (2019) compares the global average H_2O vertical profiles from previous version of ACE-FTS and MIPAS-IMK (MIPAS-IMK v5 and v20, and ACE-FTS V3.5) for the MIPAS high-resolution period (2002-2004). The obtained results exhibit a high degree of similarity to the findings reported in previous studies (Högberg et al., 2019). Coincident profile comparisons between ACE-FTS and MIPAS (IMK and ESA) reveal the presence of a minimum for both H_2O and HDO around the tropopause. Specifically, ACE-FTS demonstrates a global minimum for H_2O at 15 km, with a concentration of 4.02 ± 0.72 ppmv, while MIPAS-IMK exhibits a similar minimum at 15 km, with a concentration of 4.28 ± 0.69 ppmv. In the case of ACE-FTS and MIPAS-ESA, MIPAS-ESA displays a distinct minimum at 13 km, measuring 4.40 ± 1.03 ppmv. Conversely, the global minimum for HDO in the coincident profiles is consistently observed at an altitude of 16 km across all cases. Specifically, ACE-FTS and MIPAS-IMK demonstrate a minimum concentration of 0.54 ± 0.13 ppbv and 0.56 ± 0.25 ppbv, respectively, while the coincident profiles of ACE-FTS and MIPAS-ESA yield a minimum of 0.53 ± 0.13 ppbv for ACE-FTS and 0.58 ± 0.24 ppbv for MIPAS-ESA.

Global mean vertical profiles of HDO, along with their standard deviations are shown for ACE-FTS and MIPAS-IMK in Fig. 3(b) and for ACE-FTS and MIPAS-ESA in Fig. 3(d). The global average results are almost identical when comparing ACE-FTS and MIPAS-IMK in the range between 15 to 50 km (Fig. 3(b)). On a global average, the MIPAS-ESA dataset is also almost identical compared to ACE-FTS in the lower stratosphere (10 to 30 km) but exhibits a dry bias compared to ACE-FTS in the upper stratosphere (i.e. between 20 to 50km, see Fig. 3(d)), although according to the uncertainties, the dry bias is not significant. The global minimum value around the tropopause for HDO coincident profiles is consistently observed at an altitude of 16 km across all databases. Specifically, ACE-FTS and MIPAS-IMK demonstrate a minimum concentration of 0.54 ± 0.13 ppbv and 0.56 ± 0.25 ppbv, respectively, while the coincident profiles of ACE-FTS and MIPAS-ESA yield a minimum of 0.53 ± 0.13 ppbv for ACE-FTS and 0.58 ± 0.24 ppbv for MIPAS-ESA. Högberg et al. (2019) also compared HDO profiles from the above-mentioned previous versions of the MIPAS-IMK and ACE-FTS. They demonstrated a high consistency in the structures along the stratosphere between the two databases. They showed a dry bias of MIPAS-IMK in the tropopause and the lower mesosphere of roughly 0.1 ppmv. In this new version of the data, the dry bias is present in comparison to ACE-FTS, but it is even more reduced.

https://doi.org/10.5194/egusphere-2023-1348
Preprint. Discussion started: 20 July 2023

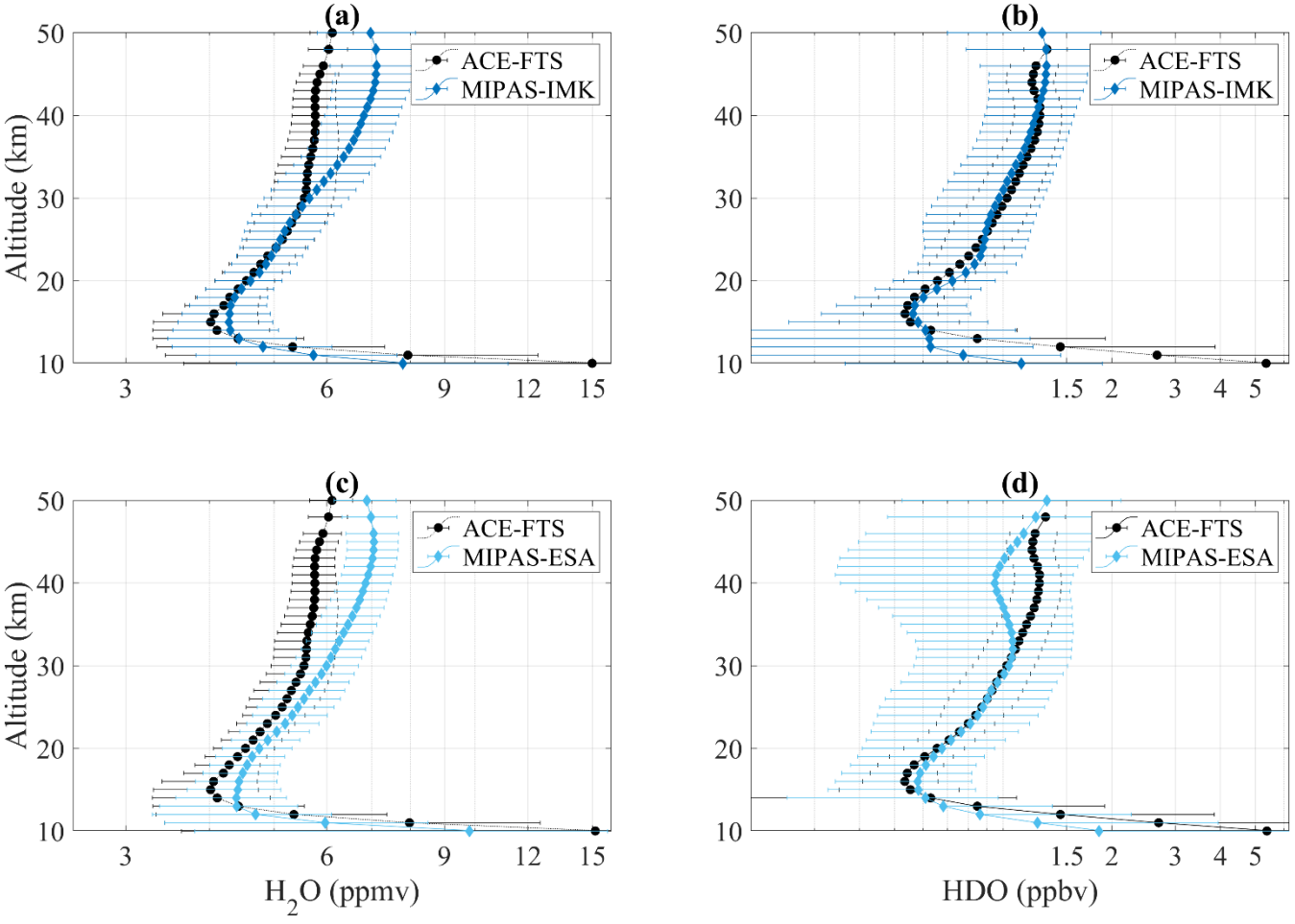

Figure 3. Global averaged vertical profiles comparison between ACE-FTS (black dots) and MIPAS-IMK (blue dots) are shown for (a) H_2O observations and (b) HDO observations. Global averaged vertical profiles comparison between ACE-FTS (black dots) and MIPAS-ESA (blue dots) are shown for (c) H_2O observations and (d) HDO observations. The error bars represent the 1σ standard deviation.

4.2. Bias comparison

Figure 4 shows the biases derived from the profile-to-profile comparisons as described in section 3.1.3. As shown above, the comparisons are typically based on several thousand coincidences above approximately 15 km, and cover latitudes from 90º S to 90° N for the 2004-2012 period.

https://doi.org/10.5194/egusphere-2023-1348
Preprint. Discussion started: 20 July 2023

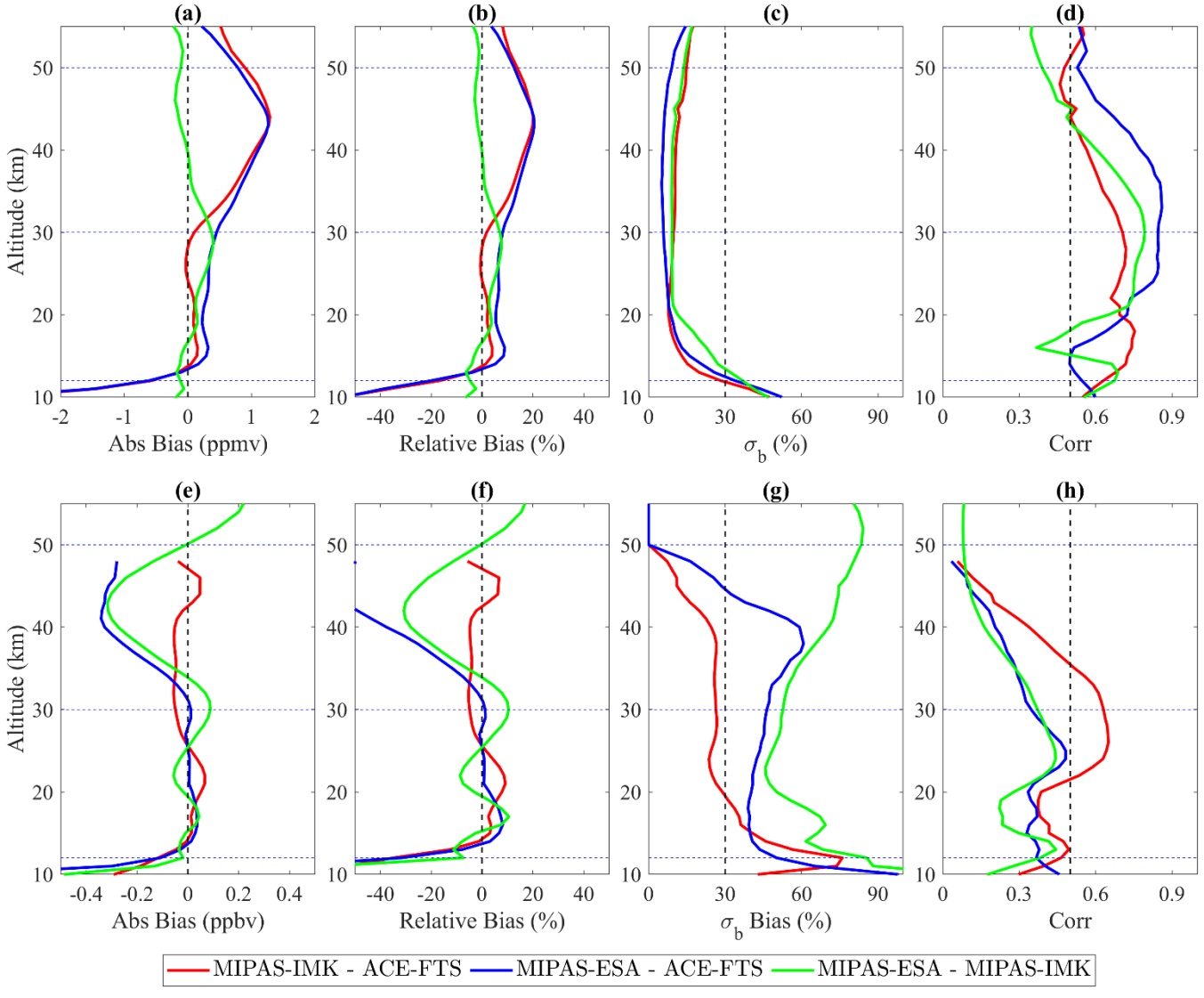

Figure 4. Comparisons between MIPAS-IMK, MIPAS-ESA and ACE-FTS for H_2O (top panels) and HDO (bottom panels): (a, e) the absolute bias, (b, f) the relative bias, (c, g) the standard deviation of the relative bias and (d, h) correlation. Black dashed lines indicate 0 ppbv, 0%, 30% and 0.5 from left to right in the different panels.

There is a good agreement in the H_2O absolute bias between 10 km and 30 km for the three databases (Fig. 4(a)). Between MIPAS (IMK and ESA) and ACE-FTS, the absolute bias reaches 1 ppmv near the 40 km region. The comparisons of the MIPAS-IMK data set with the coincident MIPAS-ESA profiles show relative biases less than 7.6 % in the middle stratosphere (close to 30 km). The relative biases observed in the three analyzed cases for the lower stratosphere (10-30 km) are all below 8.9 %, as depicted in Fig. 4(b). Beyond the altitude of 30 km, the relative biases in the comparisons with the ACE-FTS data

https://doi.org/10.5194/egusphere-2023-1348
Preprint. Discussion started: 20 July 2023

set exhibit values exceeding 9.0 %, increasing with altitude until reaching approximately the 40 km region, where the bias starts to decrease. Figure 4(c) shows the comparison between the H_2O debiased standard deviations of H_2O obtained by comparing the data sets. All the results show a good agreement and small variations in all the stratosphere. The correlation coefficients are always positive and almost always greater than 0.5 (Fig. 4(d)). Lower correlation coefficients (0.37) are observed in the 15 km to 18 km altitude range in the MIPAS-IMK and MIPAS-ESA comparisons, related to higher standard deviation values (22.6 %).

HDO absolute bias varies from -0.56 to 0.07 ppbv in the 16 to 30 km altitude range (Fig. 4(e)). The relative bias for HDO ranges from -8.7 to 9.2 % (Fig. 4(f)) between the same altitudes. The HDO debiased standard deviations (Fig. 4(g)) shows values of 50 % and higher in the comparisons using MIPAS-ESA. The lowest correlation coefficients (below of 0.44) are also found for MIPAS-ESA comparisons (Fig. 4(h)), with a minimum correlation of 0.23 and 1-σ of 69.4 % in the range between 15 and 18 km.

In accordance with previous comparisons by Högberg et al. (2019) between MIPAS-IMK and ACE-FTS datasets, relative biases for H_2O were found to be smaller than 10.0 %. However, in our current study, deviations show an increasing trend beyond 35 km, reaching a maximum value of 20.1 % at 44 km. For HDO, the relative biases remain below 10.0 %, which is consistent with the findings of Högberg et al. (2019). Moreover, the comparison reveals similar behavior below 12 km and above 35 km, where the relative biases exceed the 10.0 % threshold. For MIPAS-ESA, Raspollini et al. (2020) also showed the HDO mean absolute and relative bias between MIPAS-ESA and ACE-FTS v4.1/4.2 data. However, they use different coincidence criteria for the determination of coincident profiles, and then, their results are not directly comparable.

Tables 1 and 2 summarise the global average characteristics of the H_2O and HDO comparisons between 16 to 30 km (from the tropical tropopause to the middle stratosphere) for the period 2004-2012. The results come from coincident profiles for the full globe without latitude restriction.

Table 1. H_2O range of the statistical quantities for the comparison of the databases between 16 to 30 km of altitude for the full globe. From left to right: the mean absolute bias, the mean relative bias, the debiased standard deviation and the correlation coefficient.

	Bias Abs. H_2O (ppmv)	Bias Rel. H_2O (%)	1σ Bias H_2O (%)	Corr.
MIPAS-IMK vs ACE-FTS	- 0.03 - 0.15	- 0.7 - 4.0	7.7 - 11.1	0.69 - 0.75
MIPAS-ESA vs ACE-FTS	0.22 - 0.45	5.4 - 8.9	5.8 - 13.0	0.51 - 0.85
MIPAS-ESA vs MIPAS-IMK	- 0.06 - 0.40	- 1.7 - 7.6	9.1 - 22.6	0.37 - 0.79

https://doi.org/10.5194/egusphere-2023-1348
Preprint. Discussion started: 20 July 2023

Table 2. HDO range of the statistical quantities for the comparison of the databases between 16 to 30 km of altitude for the full globe. From left to right: the mean absolute bias, the mean relative bias, the debiased standard deviation and the correlation coefficient.

	Bias Abs. HDO (ppbv)	Bias Rel. HDO (%)	1σ Bias HDO (%)	Corr.
MIPAS-IMK vs ACE-FTS	-0.05 - 0.07	- 4.9 - 9.2	23.7 - 36.2	0.37 - 0.65
MIPAS-ESA vs ACE-FTS	- 0.01 - 0.04	- 1.0 - 8.1	39.0 - 46.4	0.33 - 0.48
MIPAS-ESA vs MIPAS-IMK	- 0.06 - 0.09	- 8.7 - 10.6	45.9 - 69.4	0.22 - 0.44

The relative biases in the lower stratosphere show a difference of less than 8.9 % but higher than -1.7 % for H_2O (Table 1) as shown in the Fig. 4. The comparison between MIPAS-IMK and ACE-FTS has a 1-σ standard deviation within the range of 7.7 to 11.1 %, and a maximum correlation of 0.75. On the other hand, the average difference between MIPAS-ESA and ACE-FTS in the lower stratosphere is ranging 5.4 to 8.9 %, exhibiting a wet bias and well within the 1-σ standard deviation of 5.8 to 3.0 % and has a maximun correlation coefficient of 0.85. Finally, quantifying the H_2O differences between MIPAS-ESA and MIPAS-IMK in the lower levels of the stratosphere, a dry bias of 1.7 % was observed at an altitude of 16 km. Within lower stratosphere region, the relative bias exhibited a range of - 1.7 to 7.6 %, well within the 1-σ standard deviation of 22.6 % in the range of 9.1 to 22.6 % and a correlation coefficient of 0.37 at 16 km. The correlations in the lower levels of the stratosphere were between 0.37 to 0.79.

For HDO (Table 2) the mean absolute bias is much smaller for the three databases in the lower stratosphere and the relative bias is between - 8.7 to 10.6%. In contrast to H_2O, the debiased standard deviation ranges are far larger with values between 23.7 and 69.4 %, and the correlation coefficients are lower, between 0.22 to 0.65.

4.3. Comparisons of seasonally averaged latitude cross-sections

Figure 5 shows the seasonally averaged latitude-pressure cross sections of H_2O and HDO for the three data sets considered in the comparisons from 90º S to 90° N. Water shows a large depletion in the tropopause in the three data sets both in JJA (Fig. 5(a)) and DJF (Fig. 5(b)), with values between 3-5 ppmv in the lower stratosphere. In Antarctica, the H_2O and HDO values in the polar winter vortex is less than 2.9 ppmv and 0.33 ppbv, respectively. These low values evidence the effect of dehydration through the formation of PSCs. The depletion in the tropics occurs at a higher altitude than in the mid-latitudes. A secondary minimum in the tropical middle stratosphere is also appreciated in both seasons, associated with the minimum originating in the lower stratosphere during the previous year and propagated upward by the Brewer-Dobson circulation. ACE-FTS might even show a third minimum, at least for DJF. This ascent rate of water vapor in the tropical lower stratosphere by the upwelling branch of the Brewer-Dobson circulation imprint a seasonal cycle of H_2O known as the atmospheric tape recorder (Mote et al., 1996) as will be seen in the next section. With increasing altitude, an increase in H_2O is found to be consistent with the

https://doi.org/10.5194/egusphere-2023-1348
Preprint. Discussion started: 20 July 2023

global mean vertical profiles shown in Fig. 3. Higher values of H_2O are found first over high latitudes in the summer hemisphere reflecting the production of WV through methane oxidation under a long duration of sunlight (LeTexier et al., 1988). In general, H_2O shows in the zonal mean the expected distribution that has been established in previous studies (e.g., Randel et al., 2001). The general distribution of HDO (Fig.s 5(c) and 5(d)) shows some similarities to that of H_2O (Fig. 5(a) and 5(b)), reflecting that both species have a common in situ source in the stratosphere, i.e., oxidation of CH_4 and H_2.

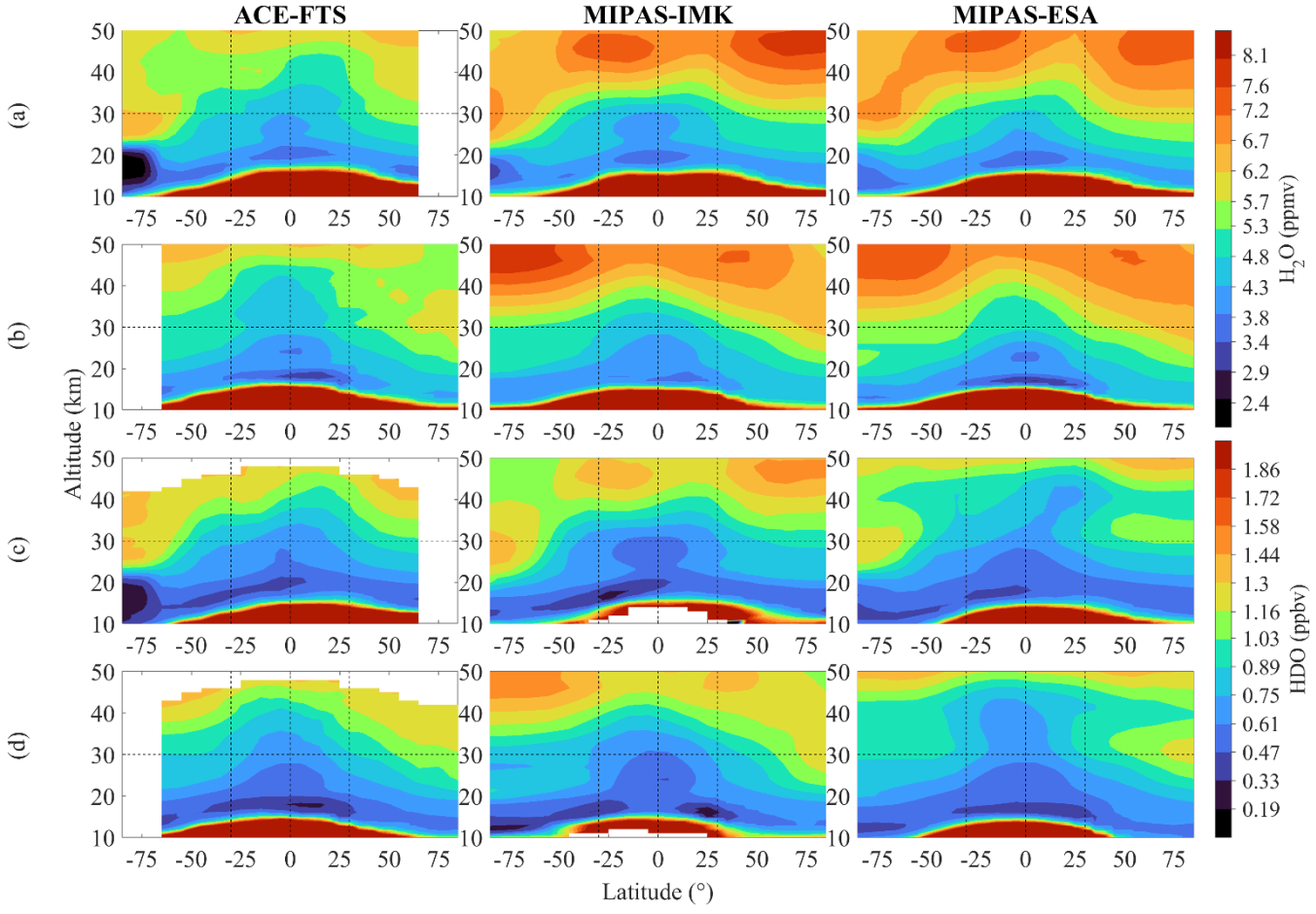

Figure 5. Meridional cross-sections of H_2O in (a) summer and (b) winter, of HDO for (c) summer and (d) winter for three datasets. The left column represents ACE-FTS data, the middle column represents the MIPAS-IMK data and the right column the MIPAS-ESA data. The climatology is based on the 2004-2012 period. The absence of profiles inMIPAS- IMK map below the tropical tropopause is due to a more stringent cloud filtering approach used by IMK.

The changes in δD mirror changes in H_2O and HDO in the stratosphere (Fig. 6). Above the climatological tropopause, a large depletion in δD is found in the three datasets. During the boreal summer, the latitudinal gradient in δD due to atmospheric dynamics associated with the polar vortex can be distinguished (Fig. 6(a)). However, there is still a relative minimum in δD

https://doi.org/10.5194/egusphere-2023-1348
Preprint. Discussion started: 20 July 2023

near the tropopause in all latitudes. A secondary minimum about 30 km in the tropical stratosphere is more clearly observed in MIPAS-IMK data and MIPAS-ESA data than in ACE-FTS data, both for summer (Fig. 6(a)) and winter (Fig. 6(b)). Finally, in MIPAS-ESA data, the air above 30 km is not enriched in deuterium as in the other two databases. It is known that the oxidation of methane in the stratosphere should cause an increase in the isotopic ratio, as water vapour transported from the troposphere to the stratosphere is stronger depleted in the heavier isotopologues (Wang et al. 2018). The results obtained with δD for ACE-FTS are in agreement with Randel et al. (2012) results from previous data versions (2004 to 2009). δD for MIPAS-IMK is partially in agreement with Högberg et al. (2019), these authors also observed two minima in the lower stratosphere in previous version (2002 to 2004), but the minima in Högberg et al. (2019) are less intense than the result in Fig. 6 at 25° S.

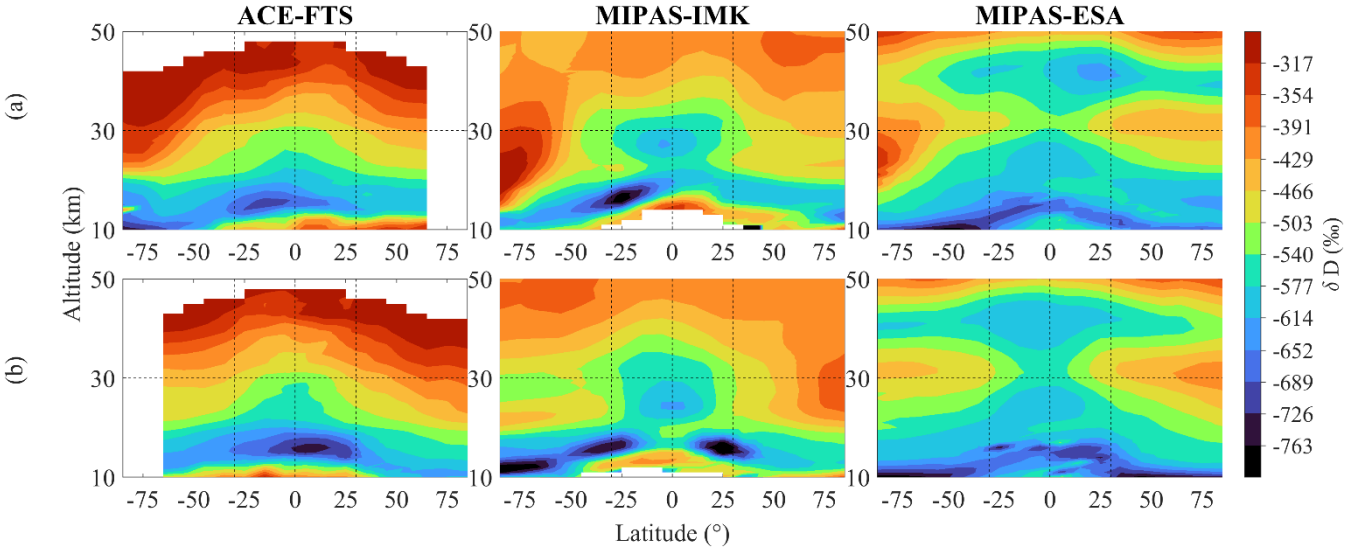

Figure 6. Meridional cross-sections of δD in (a) summer (JJA) and (b) winter (DJF) for the three datasets. The left column represented ACE-FTS data, the middle column the MIPAS-IMK data and the right column the MIPAS-ESA data. The climatology is based on the 2004-2012 period. Data gaps are indicated by white areas; in MIPAS-IMK they are related to the strict cloud-clearing algorithm used to retrieve data.

4.4. Comparison of the tropical seasonal cycle

Several details of the vertical propagation of the tropical seasonal signal and the interannual variability of the three databases are shown in Fig. 7, which depicts the height-time diagrams over 30º S and 30º N of H_2O (left panels) and HDO (right panels) concentrations. Figures 7(a), 7(b) and 7(c) show minimum annual values in H_2O and HDO originating near the tropical tropopause and propagating vertically to above 25 km, which is known as the tape recorder signature (Mote et al., 1996). The interannual variability in ACE-FTS data ((Fig. 7(a)) and MIPAS-IMK ((Fig. 7(b)) data are more similar between them to the MIPAS-ESA interannual variability ((Fig. 7(c)).

https://doi.org/10.5194/egusphere-2023-1348
Preprint. Discussion started: 20 July 2023

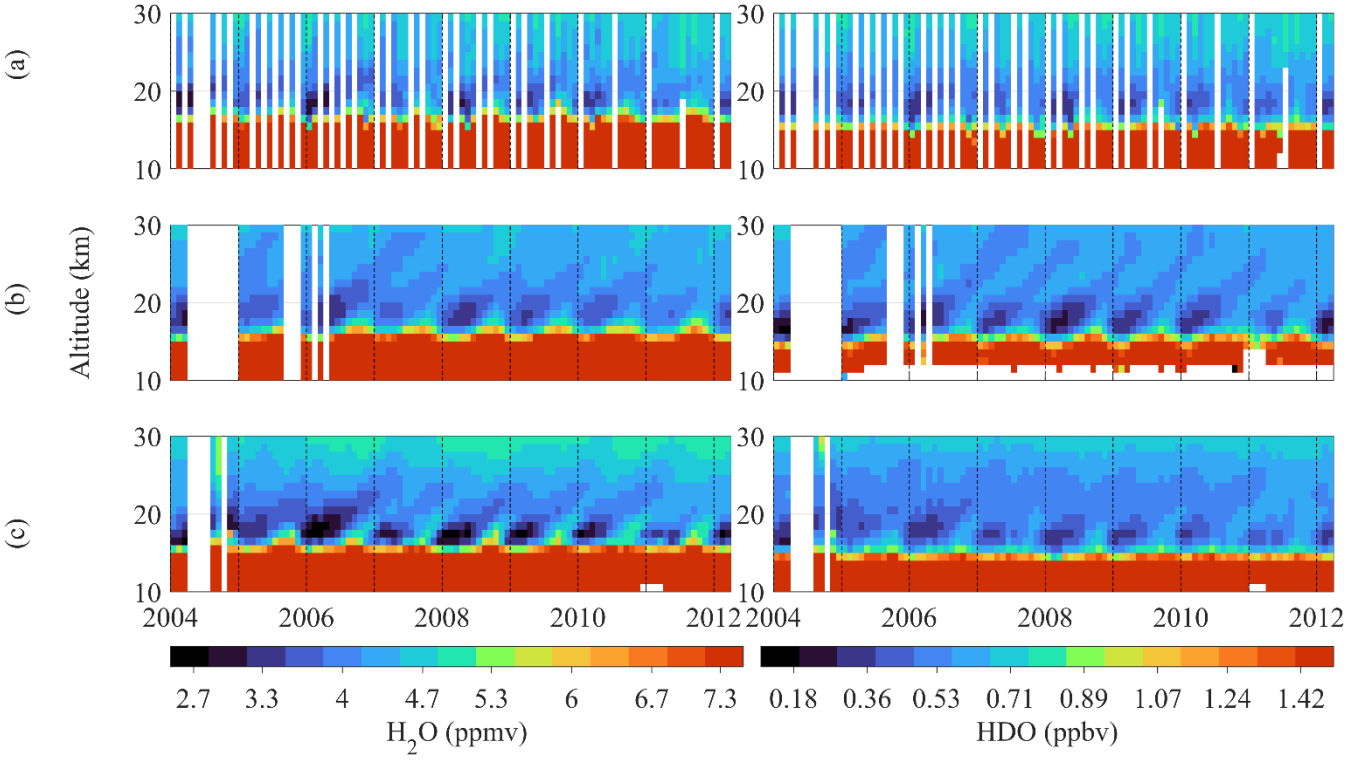

Figure 7. Altitude vs. time diagrams over 30° S and 30° N of H_2O and HDO VMR for the datasets (a) ACE-FTS, (b) MIPAS-IMK, and (c) MIPAS-ESA. White color indicates data gaps.

455

The altitude-time variability of δD is depicted in Fig. 8. ACE-FTS data (Fig. 8(a)) show small annual fluctuations in the lower stratosphere though it shows the characteristic tape recorder pattern of the annual δD minimum. By contrast, in MIPAS-IMK, the annual variation related to the tape recorder signature is evident (Fig. 8(b)). Lossow et al. (2020) showed that a tape recorder signal exists in ACE-FTS version 3.5 data as well, although with a lower seasonal amplitude of ~ 25 ‰ in contrast to MIPAS-
460 IMK δD data, that have (in the data version investigated there) a seasonal amplitude of about 75 ‰. Figure 8 demonstrates that the differences in seasonal amplitudes found for older data versions remain for the most recent data versions. Finally, MIPAS-ESA show a minimum in the lower stratosphere with low vertical propagation.

In the troposphere near to 14 km, a deuterium depletion (compared to SMOW) of -560 ‰ is observed for MIPAS-ESA, -420
465 ‰ for ACE-FTS and -470‰ for MIPAS-IMK. As it was previously shown in the Fig.3, the MIPAS instrument shown a negative bias at the troposphere, while the ACE-FTS instrument can measure with higher sensitivity further down in the atmosphere, reaching the upper middle part of the troposphere. For this reason, it is most likely that the ACE-FTS database shows more realistic values of the δD distribution at these altitudes compared to the other instrument.

https://doi.org/10.5194/egusphere-2023-1348
Preprint. Discussion started: 20 July 2023

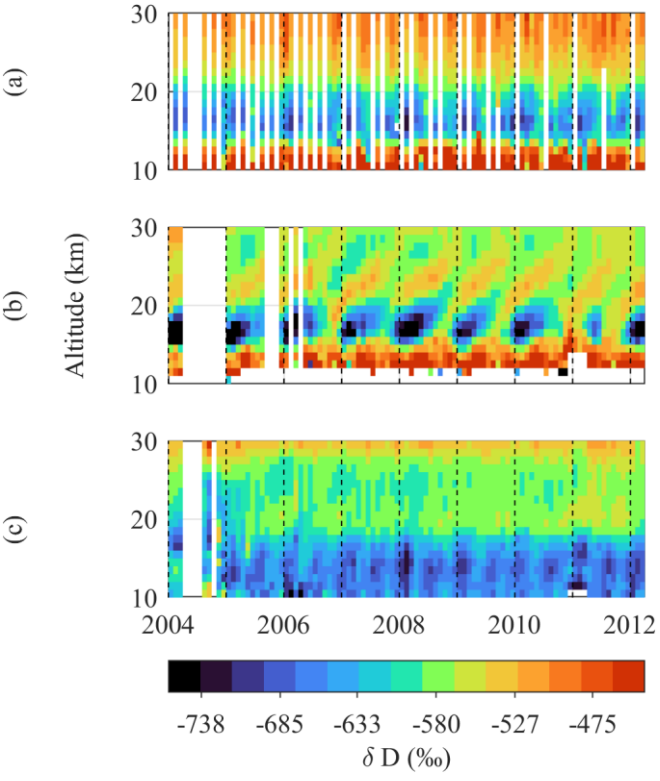

Figure 8. Height-time diagrams of δD in the 30° S-30° N band derived from (a) ACE-FTS observations, (b) MIPAS-IMK observations and (c) MIPAS-ESA observations during 2004-2012.

In Fig. 8, there is a steep vertical gradient in the troposphere for both MIPAS-IMK and ACE-FTS. The dry δD in MIPAS-IMK and ACE-FTS between 14 to 20 km are between -730 to -680 ‰ and -680 to -620 ‰. For MIPAS-ESA I see up to ~18 km mostly blue values around -560 ‰.

5. SUMMARY AND CONCLUSIONS

This work presents H_2O, HDO and δD comparisons among 3 data sets of stratospheric and lower mesospheric data from two different satellite instruments, ACE-FTS and MIPAS. The recent data versions ACE-FTS V4.1/4.2, MIPAS-IMK V5H_H2O_20, V5R_H2O_220/221, V5H_HDO_22 and V5R_H2O_222/223 and MIPAS-ESA Level 2 V8 were compared. Specifically, the comparison with MIPAS-ESA is performed for the first time in this work for the period 2004 - 2012. The database comparison is based on two approaches: profile-to-profile comparisons, and climatology comparisons not requiring coincidences of the observations. The main conclusions of this study are summarized as follows:

The vertical behavior of H_2O profiles between 16 and 30 km altitude levels shows remarkable similarity between ACE-FTS and MIPAS-IMK, with only minor differences observed between ACE-FTS and MIPAS-ESA within these altitudes.

https://doi.org/10.5194/egusphere-2023-1348
Preprint. Discussion started: 20 July 2023

Discrepancies can be observed above 30 km in MIPAS (IMK and ESA) vs ACE-FTS, but according to the uncertainties, they are not significant. The global HDO profiles are almost identical when comparing ACE-FTS and MIPAS-IMK. In the case of MIPAS-ESA, a negative difference is depicted in the upper levels of the stratosphere, but it is within the 1-σ standard deviation of the global average coincident profiles. The analysis conducted in this study highlights a higher level of agreement in HDO measurements obtained from ACE-FTS in both comparison cases. These findings contribute to our understanding of the agreement and discrepancies among the datasets analyzed in this study. The results are quite similar to those obtained by Högberg et al. (2019) for previous versions of MIPAS-IMK and ACE-FTS for the period 2002-2004.

Biases from profile-to-profile comparisons exhibited the quantitaty differences between the global average profiles. H_2O biases in the lower stratosphere (16 km to 30 km) ranged from -1.6 % to 8.9 % across the three databases. The largest biases were found just above 35 km in MIPAS (ESA and IMK) vs ACE-FTS comparisons, reaching maximum deviations of 20.1 % and 20.5 % at 43 km (ESA) and 44 km (IMK) respectively. The 1-σ standard deviation among the databases ranged from 5.7 % to 22.6 %. Correlation coefficients were mostly above 0.5, except for MIPAS-IMK vs MIPAS-ESA comparisons in the upper troposphere and lower mesosphere. The HDO biases observed within 16 km and 30 km exhibit reduced variability and consistently remain below 10.6 %. Specifically, when comparing HDO measurements between ACE-FTS and MIPAS-IMK, a positive bias of less than 10.2 % and a negative bias exceeding -2.9 % are observed. HDO biases agreed with Högberg et al. (2019), ranging from -8.7 % to 10.6 % in MIPAS-IMK vs ACE-FTS. For MIPAS-ESA, Raspollini et al. (2020) used a different method for coincident profile determination, making direct comparisons of HDO biases with our study unfeasible. In terms of combined precision and Pearson correlation coefficient, comparisons involving MIPAS-ESA showed poorer performance compared to MIPAS-IMK and ACE-FTS. Lower correlation and higher 1-σ values were observed in the 14 km to 17 km altitude range, which corresponds to the tropical tropopause region.

We also overviewed meridional cross sections in the three databases. Consistent with previous observations, the overall vertical structure of H_2O and HDO exhibits a large depletion near the tropopause and a secondary minimum above in the tropical region and an increase in H_2O and HDO with altitude because of the methane oxidation. An exception here for HDO is the MIPAS-ESA data set which shows the secondary minimum in HDO at higher altitudes than in MIPAS-IMK and ACE-FTS. MIPAS-ESA practically doesn't show the HDO increase at high latitudes and altitudes. The vertical structure of δD is in good agreement with previous versions of MIPAS-IMK and ACE-FTS data (Randel et al., 2012; Högberg et al., 2019). Latitude-altitude sections of δD for MIPAS-ESA have never been shown before and they exhibit distinct discrepancies with the other two databases.

Finally, the general depiction of the tape recorder signal in H_2O and HDO for the three databases seems to be reasonable. However, the temporal variations in stratospheric δD show different signals. MIPAS-ESA depicts minimal variations in δD in

https://doi.org/10.5194/egusphere-2023-1348
Preprint. Discussion started: 20 July 2023

the lower stratosphere with some short vertical propagations each year. ACE-FTS shows slight discrepancies with MIPAS-IMK as in the previous versions of the data (Randel et al., 2012).

In conclusion, the lack of complete agreement among the three databases presents challenges in reaching definitive conclusions. Nevertheless, the findings from this study suggest that the MIPAS-IMK dataset provides a more realistic signal for the entire stratosphere. However, it is crucial to exercise caution when interpreting these results, specifically considering the sampling limitations of ACE-FTS in the tropics, during the period of study, especially at lower altitudes.

Code availability

The code in MATLAB is available from the authors upon request.

Data availability

The MIPAS-IMK H_2O dataset can be accessed from the website of the Institute of Meteorology and Climate Research / Atmospheric Trace Gases and Remote Sensing Division (IMK-ASF) at https://www.imk-asf.kit.edu/english/308.php. For HDO data, information can be obtained upon request. The ACE-FTS data can be accessed and downloaded from the website https://databace.scisat.ca/level2. The MIPAS-ESA data is available online and can be downloaded from the FTP server ftp://mip-ftp-ds.eo.esa.int/ using an FTP client.

Author contribution:

L.A. P.O and G.P.S. conceived and designed the research. K.DLR. developed the analysis. P.O and K.DLR. prepared the manuscript draft. K.DLR., P.O., G.P.S. M.K., P.R., M.G., K.A.W., C.P-O. and L.A. reviewed and edited the manuscript. All authors have read and agreed to the published version of the manuscript.

Competing interests:

One of the authors (G.P.S.) is associate editor of AMT.

Acknowledgements

https://doi.org/10.5194/egusphere-2023-1348
Preprint. Discussion started: 20 July 2023

This research has been supported by the following grants: the Spanish Ministerio de Economía y Competitividad (grant no. CGL2016-78562-P), PAPIIT (DGAPA-UNAM) IN116120, IG101423 and CONACyT 315839. Paulina Ordoñez is grateful for the support of Maria Zambrano (UPO, Ministry of Universities, Recovery, Transformation and Resilience Plan -Funded by the European Union -Next Generation EU). The Atmospheric Chemistry Experiment (ACE) is a Canadian-led mission mainly supported by the CSA and the NSERC, and Peter Bernath is the principal investigator. The IMK team would like to thank the European Space Agency for making the MIPAS level-1b data set available. We acknowledge Michael Kiefer for his assistance with IMK data management and providing comments during the early phase of the manuscript. Karen de los Rios is grateful to the National Council on Science and Technology (CONACYT) for their generous financial support and scholarship. Special appreciation is extended to J. R. Torres-Castillo for his invaluable assistance in enhancing the employed algorithms. Additionally, Karen de los Rios acknowledges R. Stanley Molina-Garza for his insightful recommendations.

References

Bernath, P. F., McElroy, C. T., Abrams, M. C., Boone, C. D., Butler, M., Camy-Peyret, C., Carleer, M., Clerbaux, C., Coheur, P.-F., Colin, R., DeCola, P., DeMazière, M., Drummond, J. R., Dufour, D., Evans, W. F. J., Fast, H., Fussen, D., Gilbert, K., Jennings, D. E., Llewellyn, E. J., Lowe, R. P., Mahieu, E., McConnell, J. C., McHugh, M., McLeod, S. D., Michaud, R., Midwinter, C., Nassar, R., Nichitiu, F., Nowlan, C., Rinsland, C. P., Rochon, Y. J., Rowlands, N., Semeniuk, K., Simon, P., Skelton, R., Sloan, J. J., Soucy, M.-A., Strong, K., Tremblay, P., Turnbull, D., Walker, K. A., Walkty, I., Wardle, D. A., Wehrle, V., Zander, R., and Zou, J.: Atmospheric chemistry experiment (ACE): Mission overview, Geophys. Res. Lett., 32, 1–5, https://doi.org/10.1029/2005GL022386, 2005.

Boone, C. D., Nassar, R., Walker, K. A., Rochon, Y., McLeod, S. D., Rinsland, C. P., and Bernath, P. F.: Retrievals for the atmospheric chemistry experiment Fourier-transform spectrometer, Appl. Opt., 44, 7218–7231, https://doi.org/10.1364/AO.44.007218, 2005.

Boone, C. D., Walker, K. A., and Bernath, P. F.: Version 3 retrievals for the atmospheric chemistry experiment Fourier transform spectrometer (ACE-FTS), The Atmospheric Chemistry Experiment ACE at 10: A Solar Occultation Anthology, A. Deepak Publishing, Hampton, Va., 2013.

Boone, C. D., Bernath, P. F., Cok, D., Jones, S. C., and Steffen, J.: Version 4 retrievals for the atmospheric chemistry experiment Fourier transform spectrometer (ACE-FTS) and imagers. Journal of Quantitative Spectroscopy and Radiative Transfer, 247, 106939, https://doi.org/10.1016/j.jqsrt.2020.106939, 2020.

Brewer, A. W.: Evidence for a world circulation provided by the measurements of helium and water vapour distribution in the stratosphere. Quarterly Journal of the Royal Meteorological Society, 75, 351–363, https://doi.org/10.1002/qj.49707532603, 1949.

https://doi.org/10.5194/egusphere-2023-1348
Preprint. Discussion started: 20 July 2023

Ceccherini, S., Carli, B., Raspollini, P., and Ridolfi, M.: Rigorous determination of stratospheric water vapor trends from MIPAS observations, Optics Express, 19(S3), A340-A360, https://doi.org/10.1364/OE.19.00A340, 2011.

von Clarmann, T., Glatthor, N., Grabowski, U., Höpfner, M., Kellmann, S., Kiefer, M., Linden, A., Tsidu, G. M., Milz, M., Steck, T., Stiller, G. P., Wang, D. Y., Fischer, H., Funke, B., Gil-López, S., and López-Puertas, M.: Retrieval of temperature and tangent altitude pointing from limb emission spectra recorded from space by the Michelson Interferometer for Passive Atmospheric Sounding (MIPAS). J. Geophys. Res. Atmos., 108(D23), 4719. https://doi.org/10.1029/2003jd003602, 2003.

von Clarmann, T., Höpfner, M., Kellmann, S., Linden, A., Chauhan, S., Funke, B., Grabowski, U., Glatthor, N., Kiefer, M., Schieferdecker, T., Stiller, G. P., and Versick, S.,: Retrieval of temperature, H2O, O3, HNO3, CH4, N2O, ClONO2 and ClO from MIPAS reduced resolution nominal mode limb emission measurements. Atmos. Meas. Tech., 2(1), 159-175. https://doi.org/10.5194/amt-2-159-2009, 2009.

Von Clarmann, T.: Validation of remotely sensed profiles of atmospheric state variables: strategies and terminology. Atmos. Chem. Phys., 6, 4311-4320, https://doi.org/10.5194/acp-6-4311-2006, 2006.

Dessler, A. E., Schoeberl, M. R., Wang, T., Davis, S. M., and Rosenlof, K. H.: Stratospheric water vapor feedback. Proc. Natl. Acad. Sci. U. S. A., 110, 18087–18091, https://doi.org/10.1073/pnas.1310344110, 2013.

Dinelli, B. M., Raspollini, P., Gai, M., Sgheri, L., Ridolfi, M., Ceccherini, S., Barbara, F., Zoppetti, N., Castelli, E., Papandrea, E., Pettinari, P., Dehn, A., Dudhia, A., Kiefer, M., Piro, A., Flaud, J. M., López-Puertas, M., Moore, D., Remedios, J., and Bianchini, M.: The ESA MIPAS/ENVISAT Level2-v8 dataset: 10 years of measurements retrieved with ORM v8.22. Atmospheric Measurement Techniques Discussions, (March 2004), 1–36, https://doi.org/10.5194/amt-2021-215, 2021.

Fischer, H., Birk, M., Blom, C., Carli, B., Carlotti, M., von Clarmann, T., Delbouille, L., Dudhia, A., Ehhalt, D., Endemann, M., Flaud, J. M., Gessner, R., Kleinert, A., Koopman, R., Langen, J., López-Puertas, M., Mosner, P., Nett, H., Oelhaf, H., Perron, G., Remedios, J., Ridolfi, M., Stiller, G., and Zander, R.: MIPAS: An instrument for atmospheric and climate research. Atmospheric Chemistry and Physics, 8(8), 2151–2188, https://doi.org/10.5194/acp-8-2151-2008, 2008.

Froidevaux, L., Livesey, N.J., Read, W.G., Jiang, Y.B., Jimenez, C., Filipiak, M.J., Schwartz, M.J., Santee, M.L., Pumphrey, H.C., Jiang, J.H., Wu, D.L., Manney, G.L., Drouin, B.J., Waters, J.W., Fetzer, E.J., Bernath, P.F., Boone, C.D., Walker, K.A., Jucks, K.W., Toon, G.C., Margitan, J.J., Sen, B., Webster, C.R., Christensen, L.E., Elkins, J.W., Atlas, E., Lueb, R.A., and Hendershot, R.: Early validation analyses of atmospheric profiles from EOS MLS on the Aura satellite. IEEE Transactions on Geoscience and Remote Sensing, 44(5), 1106–1121, https://doi.org/10.1109/TGRS.2006.864366, 2006.

Gettelman, A., Birner, T., Eyring, V., Akiyoshi, H., Bekki, S., Brühl, C., Dameris, M., Kinnison, D. E., Lefevre, F., Lott, F., Mancini, E., Pitari, G., Plummer, D. A., Rozanov, E., Shibata, K., Stenke, A., Struthers, H., and Tian, W.: The Tropical Tropopause Layer 1960–2100, Atmos. Chem. Phys., 9, 1621–1637, https://doi.org/10.5194/acp-9-1621-2009, 2009.

Gordon, I.E., Rothman, L.S., Hill, C., Kochanov, R.V., Tan, Y., Bernath, P.F., Birk, M., Boudon, V., Campargue, A., Chance, K.V., Drouin, B.J., Flaud, J.-M., Gamache, R.R., Hodges, J.T., Jacquemart, D., Perevalov, V.I., Perrin, A., Shine, K.P., Smith, M.-A.H., Tennyson, J., Toon, G.C., Tran, H., Tyuterev, V.G., Barbe, A., Császár, A.G., Devi, V.M., Furtenbacher, T., Harrison, J.J., Hartmann, J.-M., Jolly, A., Johnson, T.J., Karman, T., Kleiner, I., Kyuberis, A.A., Loos, J., Lyulin, O.M.,

https://doi.org/10.5194/egusphere-2023-1348
Preprint. Discussion started: 20 July 2023

Massie, S.T., Mikhailenko, S.N., Moazzen-Ahmadi, N., Müller, H.S.P., Naumenko, O.V., Nikitin, A.V., Polyansky, O.L., Rey, M., Rotger, M., Sharpe, S.W., Sung, K., Starikova, E., Tashkun, S.A., Vander Auwera, J., Wagner, G., Wilzewski, J., Wcisło, P., Yu, S., and Zak, E.J.: The HITRAN2016 molecular spectroscopic database. J. Quant. Spectrosc. Radiat. Transf., 203, 3-69. ISSN 0022-4073, https://doi.org/10.1016/j.jqsrt.2017.06.038, 2017.

Haenel, F. J., Stiller, G. P., von Clarmann, T., Funke, B., Eckert, E., Glatthor, N., Grabowski, U., Kellmann, S., Kiefer, M., Linden, A., and Reddmann, T.: Reassessment of MIPAS age of air trends and variability, Atmos. Chem. Phys., 15, 13161–13176, https://doi.org/10.5194/acp-15-13161-2015, 2015.

Hanisco, T.F., Moyer, E. J., Weinstock, E. M., St. Clair, J. M., Sayres, D. S., Smith, J. B., Lockwood, R., Anderson, J. G., Dessler, A. E., Keutsch, F. N., Spackman, J. R., Read, W. G., and Bui, T. P.: Geophys. Res. Lett., 34, L04814, doi:10.1029/2006GL027899, 2007.

M. I. Hegglin, S. Tegtmeier, J. Anderson, L. Froidevaux, R. Fuller, B. Funke, A. Jones, G. Lingenfelser, J. Lumpe, D. Pendlebury, E. Remsberg, A. Rozanov, M. Toohey, J. Urban.: SPARC Data Initiative: Comparison of water vapor climatologies from international satellite limb sounders. J. Geophys. Res. Atmos., 118(20), 11,824-11,846, https://doi.org/10.1002/jgrd.50752, 2013.

Hegglin, M. I., Plummer, D. A., Shepherd, T. G., Scinocca, J. F., Anderson, J., Froidevaux, L., Funke, B., Hurst, D., Rozanov, A., Urban, J., von Clarmann, T., Walker, K. A., Wang, H. J., Tegtmeier, S., and Weigel, K.: Vertical structure of stratospheric water vapour trends derived from merged satellite data. Nat. Geosci., 7(10), 768–776, https://doi.org/10.1038/NGEO2236, 2014.

Högberg, C., Lossow, S., Khosrawi, F., Bauer, R., Walker, K. A., Eriksson, P., Murtagh, D. P., Stiller, G. P., Steinwagner, J., and Zhang, Q.: The SPARC water vapour assessment II: Profile-to-profile and climatological comparisons of stratospheric δd(H2O) observations from satellite. Atmos. Chem. Phys., 19(4), 2497–2526, https://doi.org/10.5194/acp-19-2497-2019, 2019.

Keller, W., and Borkowski, A.: Thin plate spline interpolation. J. Geod., 93, 1251–1269, https://doi.org/10.1007/s00190-019-01240-2, 2019.

Khosrawi, F., Lossow, S., Stiller, G. P., Rosenlof, K. H., Urban, J., Burrows, J. P., Damadeo, R. P., Eriksson, P., García-Comas, M., Gille, J. C., Kasai, Y., Kiefer, M., Nedoluha, G. E., Noël, S., Raspollini, P., Read, W. G., Rozanov, A., Sioris, C. E., Walker, K. A., and Weigel, K.: The SPARC water vapour assessment II: Comparison of stratospheric and lower mesospheric water vapour time series observed from satellites. Atmos. Meas. Tech., 11(7), 4435–4463. https://doi.org/10.5194/amt-11-4435-2018, 2018.

Kiefer, M., von Clarmann, T., Funke, B., García-Comas, M., Glatthor, N., Grabowski, U., Kellmann, S., Kleinert, A., Laeng, A., Linden, A., López-Puertas, M., Marsh, D. R., and Stiller, G. P.: IMK/IAA MIPAS temperature retrieval version 8: Nominal measurements. Atmos. Meas. Tech., 14(6), 4111–4138, https://doi.org/10.5194/amt-14-4111-2021, 2021.

https://doi.org/10.5194/egusphere-2023-1348
Preprint. Discussion started: 20 July 2023

Kleinert, A., Aubertin, G., Perron, G., Birk, M., Wagner, G., Hase, F., Nett, H., and Poulin, R.: MIPAS Level 1B algorithms overview: Operational processing and characterization. Atmos. Chem. Phys., 7, 1395–1406, https://doi.org/10.5194/acp-7-1395-2007, 2007.

Kleinert, A., Birk, M., Perron, G., and Wagner, G.: Level 1b error budget for MIPAS on ENVISAT. Atmos. Meas. Tech., 11, 5657–5672, https://doi.org/10.5194/amt-11-5657-2018, 2018.

Kuang, Z., Toon, G. C., Wennberg, P. O., and Yung, Y. L.: Measured HDO/H2O ratios across the tropical tropopause. Geophys. Res. Lett., 30, 1–4, https://doi.org/10.1029/2003GL017023, 2003.

Lanzante, J. R.: Resistant, robust and non-parametric techniques for the analysis of climate data: Theory and examples, including applications to historical radiosonde station data. Int. J. Climatol., 16, 1197–1226. https://doi.org/10.1002/(SICI)1097-0088(199611)16:11<1197::AID-JOC89>3.0.CO;2-L, 1996.

LeTexier, H., Solomon, S., and Garcia, R.R.: The role of molecular hydrogen and methane oxidation in the water vapour budget of the stratosphere. Q. J. R. Meteorol. Soc., 114, 281–295, https://doi.org/10.1002/qj.49711448002, 1988.

Loew, A., Bell, W., Brocca, L., Bulgin, C. E., Burdanowitz, J., Calbet, X., Donner, R. V., Ghent, D., Gruber, A., Kaminski, T., Kerr, Y., Kunhikrishnan, P., Li, Z., Miralles, D., Mistelbauer, T., Nicolai-Shaw, N., Parinussa, R., Reimer, C., Rudiger, C., Schanze, J., Schrön, M., Smith, M., Su, Z., Trigo, I. F., van der Schalie, R., Wagner, W., and Zeng, Y.: Validation practices for satellite-based Earth observation data across communities. Rev. Geophys., 55(3), 779-817, https://doi.org/10.1002/2017RG000562, 2017.

Lossow, S., Steinwagner, J., Urban, J., Dupuy, E., Boone, C. D., Kellmann, S., Linden, A., Kiefer, M., Grabowski, U., Glatthor, N., Höpfner, M., Röckmann, T., Murtagh, D. P., Walker, K. A., Bernath, P. F., von Clarmann, T., and Stiller, G. P.: Comparison of HDO measurements from Envisat/MIPAS with observations by Odin/SMR and SCISAT/ACE-FTS. Atmos. Meas. Tech., 4, 1855–1874, https://doi.org/10.5194/amt-4-1855-2011, 2011.

Lossow, S., Khosrawi, F., Kiefer, M., Walker, K. A., Bertaux, J.-L., Blanot, L., Russell, J. M., Remsberg, E. E., Gille, J. C., Sugita, T., Sioris, C. E., Dinelli, B. M., Papandrea, E., Raspollini, P., García-Comas, M., Stiller, G. P., von Clarmann, T., Dudhia, A., Read, W. G., Nedoluha, G. E., Damadeo, R. P., Zawodny, J. M., Weigel, K., Rozanov, A., Azam, F., Bramstedt, K., Noël, S., Burrows, J. P., Sagawa, H., Kasai, Y., Urban, J., Eriksson, P., Murtagh, D. P., Hervig, M. E., Högberg, C., Hurst, D. F., and Rosenlof, K. H.: The SPARC water vapour assessment II: Profile-to-profile comparisons of stratospheric and lower mesospheric water vapour data sets obtained from satellites. Atmos. Meas. Tech., 12(5), 2693–2732. https://doi.org/10.5194/amt-12-2693-2019, 2019.

Lossow, S., Högberg, C., Khosrawi, F., Stiller, G. P., Bauer, R., Walker, K. A., Kellmann, S., Linden, A., Kiefer, M., Glatthor, N., von Clarmann, T., Murtagh, D. P., Steinwagner, J., Röckmann, T., and Eichinger, R.: A reassessment of the discrepancies in the annual variation of δD-H2O in the tropical lower stratosphere between the MIPAS and ACE-FTS satellite data sets. Atmos. Meas. Tech., 13(1), 287–308. https://doi.org/10.5194/amt-13-287-2020, 2020.

https://doi.org/10.5194/egusphere-2023-1348
Preprint. Discussion started: 20 July 2023

Merlivat, L., and Nief, G.: Fractionnement isotopique lors des changements d'état solide-vapeur et liquide-vapeur de l'eau à des températures inférieures à 0°C. Tellus A Dyn. Meteorol. Oceanogr., 19, 122, https://doi.org/10.3402/tellusa.v19i1.9756, 1967.

Milz, M., von Clarmann, T., Fischer, H., Glatthor, N., Grabowski, U., Höpfner, M., Kellmann, S., Kiefer, M., Linden, A., Mengistu Tsidu, G., Steck, T., Stiller, G. P., Funke, B., López-Puertas, M., and Koukouli, M. E.: Water vapor distributions measured with the Michelson Interferometer for Passive Atmospheric Sounding on board Envisat (MIPAS/Envisat). J. Geophys. Res. Atmos., 110(24), 1–14, https://doi.org/10.1029/2005JD005973, 2005.

Mote, P. W., Rosenlof, K. H., McIntyre, M. E., Carr, E. S., Gille, J. C., Holton, J. R., Kinnersley, J. S., Pumphrey, H. C., Russell, J. M., Waters, J. W.: An atmospheric tape recorder: The imprint of tropical tropopause temperatures on stratospheric water vapor. J. Geophys. Res. Atmos., 101, 3989–4006, https://doi.org/10.1029/95JD03422, 1996.

Moyer, E. J., Irion, F. W., Yung, Y. L., and Gunson, M. R.: ATMOS stratospheric deuterated water and implications for troposphere-stratosphere transport. Geophys. Res. Lett., 23, 2385–2388, https://doi.org/10.1029/96GL01489, 1996.

Murtagh, D., Frisk, U., Merino, F., Ridal, M., Jonsson, A., Stegman, J., Witt, G., Eriksson, P., Jiménez, C., Megie, G., de la Noë, J., Ricaud, P., Baron, P., Pardo, J. R., Hauchcorne, A., Llewellyn, E. J., Degenstein, D. A., Gattinger, R. L., Lloyd, N. D., Evans, W. F. J., McDade, I. C., Haley, C. S., Sioris, C., von Savigny, C., Solheim, B. H., McConnell, J. C., Strong, K., Richardson, E. H., Leppelmeier, G. W., Kyrölä, E., Auvinen, H., and Oikarinen, L.: An overview of the Odin atmospheric mission. Can. J. Phys., 80, 309–319, https://doi.org/10.1139/p01-157, 2002.

Nassar, R., Bernath, P. F., Boone, C. D., Manney, G. L., Mcleod, S. D., Rinsland, C. P., Skelton, R., and Walker, K. A.: Stratospheric abundances of water and methane based on ACE-FTS measurements. Geophys. Res. Lett., 32, 2–6, https://doi.org/10.1029/2005GL022383, 2005.

Nedoluha, G. E., Kiefer, M., Lossow, S., Gomez, R. M., Kämpfer, N., Lainer, M., Forkman, P., Christensen, O. M., Oh, J. J., Hartogh, P., Anderson, J., Bramstedt, K., Dinelli, B. M., Garcia-Comas, M., Hervig, M., Murtagh, D., Raspollini, P., Read, W. G., Rosenlof, K., Stiller, G. P., and Walker, K. A.: The SPARC water vapor assessment II: Intercomparison of satellite and ground-based microwave measurements. Atmos. Chem. Phys., 17(23), 14543–14558, https://doi.org/10.5194/acp-17-14543-2017, 2017.

Payne, V. H., Noone, D., Dudhia, A., Piccolo, C., and Grainger, R. G.: Global satellite measurements of HDO and implications for understanding the transport of water vapor into the stratosphere. Q. J. R. Meteorol. Soc., 133, 1459–1471, https://doi.org/10.1002/qj.127, 2007.

Plaza, N. P., Podglajen, A., Peña-Ortiz, C., and Ploeger, F.: Processes influencing lower stratospheric water vapor in monsoon anticyclones: Insights from Lagrangian modeling. Atmos. Chem. Phys., 21(12), https://doi.org/10.5194/acp-21-9585-2021, 2021.

Randel, W. J., Moyer, E., Park, M., Jensen, E., Bernath, P., Walker, K., and Boone, C.: Global variations of HDO and HDO/H2O ratios in the upper troposphere and lower stratosphere derived from ACE-FTS satellite measurements. J. Geophys. Res. Atmos., 117, 1–16, https://doi.org/10.1029/2011JD016632, 2012.

Read, W. G., Stiller, G., Lossow, S., Kiefer, M., Khosrawi, F., Hurst, D., Vömel, H., Rosenlof, K., Dinelli, B. M., Raspollini, P., Nedoluha, G. E., Gille, J. C., Kasai, Y., Eriksson, P., Sioris, C. E., Walker, K. A., Weigel, K., Burrows, J. P., and Rozanov, A.: The SPARC Water Vapor Assessment II: assessment of satellite measurements of upper tropospheric humidity. Atmos. Meas. Tech., 15(11), 3377–3401, https://doi.org/10.5194/amt-15-3377-2022, 2022.

Ridolfi, M., Carli, B., Carlotti, M., von Clarmann, T., Dinelli, B. M., Dudhia, A., Flaud, J.-M., Höpfner, M., Morris, P. E., Raspollini, P., Stiller, G., and Wells, R. J.: Optimized forward model and retrieval scheme for MIPAS near-real-time data processing, Appl. Opt., 39(9), 1323–1340, https://doi.org/10.1364/AO.39.001323, 2000.

Riese, M., Ploeger, F., Rap, A., Vogel, B., Konopka, P., Dameris, M., and Forster, P.: Impact of uncertainties in atmospheric mixing on simulated UTLS composition and related radiative effects, J. Geophys. Res. Atmos., 117, 1–10, https://doi.org/10.1029/2012JD017751, 2012.

Rosenlof, K. H., Oltmans, S. J., Kley, D., Russell III, J. M., Chiou, E.-W., Chu, W. P., Johnson, D. G., Kelly, K. K., Michelsen, H. A., Nedoluha, G. E., Remsberg, E. E., Toon, G. C., and McCormick, M. P.: Stratospheric water vapor increases over the past half-century, Geophys. Res. Lett., 28(7), 1195–1198, https://doi.org/10.1029/2000GL012502, 2001.

Scheepmaker, R. A., aan de Brugh, J., Hu, H., Borsdorff, T., Frankenberg, C., Risi, C., Hasekamp, O., Aben, I., and Landgraf, J.: HDO and H2O total column retrievals from TROPOMI shortwave infrared measurements, Atmos. Meas. Tech., 9(8), 3921–3937, https://doi.org/10.5194/amt-9-3921-2016, 2016.

Schneider, A., Borsdorff, T., aan de Brugh, J., Aemisegger, F., Feist, D. G., Kivi, R., Hase, F., Schneider, M., and Landgraf, J.: First data set of H2O/HDO columns from the Tropospheric Monitoring Instrument (TROPOMI), Atmos. Meas. Tech., 13(1), 85–100, https://doi.org/10.5194/amt-13-85-2020, 2020.

Sheese, P. E., Boone, C. D., and Walker, K. A.: Detecting physically unrealistic outliers in ACE-FTS atmospheric measurements, Atmos. Meas. Tech., 8, 741–750, https://doi.org/10.5194/amt-8-741-2015, 2015.

Sheese, P. E., Walker, K. A., Boone, C. D., McLinden, C. A., Bernath, P. F., Bourassa, A. E., Burrows, J. P., Degenstein, D. A., Funke, B., Fussen, D., Manney, G. L., McElroy, C. T., Murtagh, D., Randall, C. E., Raspollini, P., Rozanov, A., Russell III, J. M., Suzuki, M., Shiotani, M., Urban, J., von Clarmann, T., and Zawodny, J. M.: Validation of ACE-FTS version 3.5 NOy species profiles using correlative satellite measurements, Atmos. Meas. Tech., 9(12), 5781–5810, https://doi.org/10.5194/amt-9-5781-2016, 2016.

Sheese, P. E., Walker, K. A., Boone, C. D., Bernath, P. F., Froidevaux, L., Funke, B., Raspollini, P., and von Clarmann, T.: ACE-FTS ozone, water vapour, nitrous oxide, nitric acid, and carbon monoxide profile comparisons with MIPAS and MLS, J. Quant. Spectrosc. Radiat. Transf., 186, 63–80, https://doi.org/10.1016/j.jqsrt.2016.06.026, 2017.

Solomon, S., Qin, D., Manning, M., Chen, Z., Marquis, K. B., Averyt, M. Tignor, M., and Miller, H. L.: Fourth assessment report of the Intergovernmental Panel on Climate Change: Important observations and conclusions, Curr. Sci., 92, 1034, 2007.

Solomon, S., Rosenlof, K. H., Portmann, R. W., Daniel, J. S., Davis, S. M., Sanford, T. J., and Plattner, G. K.: Contributions of stratospheric water vapor to decadal changes in the rate of global warming, Science, 327, 1219–1223, 10.1126/science.1182488, 2010.

Speidel, J., Stiller, G., Glatthor, N., Kiefer, M., Lossow, S., and von Clarmann, T.: Seasonal variations of stratospheric deuterated water in the Asian summer monsoon, Geophysical Research Abstracts, Vol. 20. EGU General Assembly 2018, EGU2018-14341, 2018.

Steinwagner, J., Milz, M., Von Clarmann, T., Glatthor, N., Grabowski, U., Höpfner, M., Stiller, G. P., and Röckmann, T.: HDO measurements with MIPAS, Atmos. Chem. Phys., 7, 2601–2615, https://doi.org/10.5194/acp-7-2601-2007, 2007.

Steinwagner, J., Fueglistaler, S., Stiller, G., Von Clarmann, T., Kiefer, M., Borsboom, P. P., Van Delden, A., and Röckmann, T.: Tropical dehydration processes constrained by the seasonality of stratospheric deuterated water, Nat. Geosci., 3, 262–266, https://doi.org/10.1038/ngeo822, 2010.

Stiller, G. P., von Clarmann, T., Haenel, F., Funke, B., Glatthor, N., Grabowski, U., Kellmann, S., Kiefer, M., Linden, A., Lossow, S., and López-Puertas, M.: Observed temporal evolution of global mean age of stratospheric air for the 2002 to 2010 period, Atmos. Chem. Phys., 12, 3311–3331, https://doi.org/10.5194/acp-12-3311-2012, 2012.

Raspollini, P., A. Piro, D. Hubert, A. Keppens, J.-C. Lambert, G. Wetzel, D. Moore, S. Ceccherini, M. Gai, F. Barbara, N. Zoppetti, with MIPAS Quality Working Group, MIPAS validation teams, MIPAS IDEAS+ (Instrument Data quality Evaluation and Analysis Service) team. ENVIromental SATellite (ENVISAT) MICHELSON INTERFEROMETER for PASSIVE ATMOSPHERIC SOUNDING (MIPAS). ESA Level 2 version 8.22 products - Product Quality Readme File. ESA-EOPG-EBA-TN-5, issue 1.0, 2020.

Toohey, M., and Strong, K.: Estimating biases and error variances through the comparison of coincident satellite measurements, J. Geophys. Res. Atmos., 112, 1–12, https://doi.org/10.1029/2006JD008192, 2007.

Tuinenburg, O. A., Risi, C., Lacour, J. L., Schneider, M., Wiegele, A., Worden, J., Kurita, N., Duvel, J. P., Deutscher, N., Bony, S., Coheur, P. F., and Clerbaux, C.: Moist processes during MJO events as diagnosed from water isotopic measurements from the IASI satellite, J. Geophys. Res., 120(20), 10,619-10,636, https://doi.org/10.1002/2015JD023461, 2015.

Vogel, B., Feck, T., and Groobß, J. U.: Impact of stratospheric water vapor enhancements caused by CH4 and H2O increase on polar ozone loss, J. Geophys. Res. Atmos., 116, 1–11, https://doi.org/10.1029/2010JD014234, 2011.

Walker, K. A., Sheese, P. E., and Zou, J.: Validation Studies for the Atmospheric Chemistry Experiment Fourier Transform Spectrometer (ACE-FTS), OSA Optical Sensors and Sensing Congress 2021 (AIS, FTS, HISE, SENSORS, ES), Optica Publishing Group, FTh4G.4, 2021.

Wang, T., Zhang, Q., Lossow, S., Chafik, L., Risi, C., Murtagh, D., and Hannachi, A.: Stable Water Isotopologues in the stratosphere retrieved from Odin/SMR measurements, Remote Sens., 10, https://doi.org/10.3390/rs10020166, 2018.

Wang, X., Dessler, A. E., Schoeberl, M. R., Yu, W., and Wang, T.: Impact of convectively lofted ice on the seasonal cycle of water vapor in the tropical tropopause layer, Atmos. Chem. Phys., 19, https://doi.org/10.5194/acp-19-14621-2019, 2019.

Waters, J. W., Froidevaux, L., Harwood, R. S., Jarnot, R. F., Pickett, H. M., Read, W. G., Siegel, P. H., Cofield, R. E., Filipiak, M. J., Flower, D. A., Holden, J. R., Lau, G. K., Livesey, N. J., Manney, G. L., Pumphrey, H. C., Santee, M. L., Wu, D. L., Cuddy, D. T., Lay, R. R., Loo, M. S., Perun, V. S., Schwartz, M. J., Stek, P. C., Thurstans, R. P., Boyles, M. A., Chandra, K. M., Chavez, M. C., Gun-Shing Chen, Chudasama, B. V., Dodge, R., Fuller, R. A., Girard, M. A., Jiang, J. H., Yibo Jiang,

https://doi.org/10.5194/egusphere-2023-1348
Preprint. Discussion started: 20 July 2023

Knosp, B. W., LaBelle, R. C., Lam, J. C., Lee, K. A., Miller, D., Oswald, J. E., Patel, N. C., Pukala, D. M., Quintero, O., Scaff, D. M., Van Snyder, W., Tope, M. C., Wagner, P. A., and Walch, M. J.: The Earth Observing System Microwave Limb Sounder (EOS MLS) on the aura satellite, IEEE Trans. Geosci. Remote Sens., 44(5), 1075–1092, https://doi.org/10.1109/TGRS.2006.873771, 2006.

Wetzel, G., Oelhaf, H., Berthet, G., Bracher, A., Cornacchia, C., Feist, D. G., Fischer, H., Fix, A., Iarlori, M., Kleinert, A., Lengel, A., Milz, M., Mona, L., Müller, S. C., Ovarlez, J., Pappalardo, G., Piccolo, C., Raspollini, P., Renard, J.-B., Rizi, V., Rohs, S., Schiller, C., Stiller, G., Weber, M., and Zhang, G.: Validation of MIPAS-ENVISAT H2O operational data collected between July 2002 and March 2004, Atmos. Chem. Phys., 13(11), 5791-5811, https://doi.org/10.5194/acp-13-5791-2013, 2013.